POLITECNICO DI MILANO

School of Industrial and Information Engineering
Master of Science in Electrical Engineering

Cogging Torque and Torque ripple analysis of Permanent Magnet Synchronous machines

Supervisor:

Prof. Antonino Di Gerlando

Master Thesis by:

Shainu Sunilkumar

Student ID number:

10599259

Academic Year: 2019/2020

ACKNOWLEDGEMENT

Foremost, I would like to express my sincere thanks to my academic Supervisor, Prof. Antonino Di Gerlando for his patience, motivation and continuous support of my thesis work. I extend my sincerity towards all the faculties of the School of Industrial and Information Engineering, Politecnico Di Milano, for all the considerate guidance.

I take immense pleasure in expressing my gratitude towards my parents for being the backbone of my life. I am grateful to my family and friends for always encouraging me to go beyond limits.

It is a pleasure to acknowledge my deepest thanks to everyone who supported me throughout the course. Finally, I thank the Almighty for His grace and blessings.

எண்ணிய எண்ணியாங்கு எய்துப எண்ணியார்
திண்ணிய ராகப் பபறின்.

- திருவள்ளுவர்

Table of Contents

LIST OF FIGURES..... III
LIST OF TABLES..... V
LIST OF SYMBOLS..... VI

CHAPTER 1: PERMANENT MAGNET SYNCHRONOUS MACHINES.....3

1.1 Introduction.....3
1.2 Construction of Permanent magnet Synchronous machines.....3
1.3 Working of PM Synchronous machines.....6
1.4 Applications of PMSMs.....8
1.5 Advantages of permanent magnet synchronous motor.....9
1.6 Drawbacks of permanent magnet synchronous motor.....9
1.7 Conclusion.....9

CHAPTER 2: PMSM ANALYSIS OF TORQUE RIPPLE, NOISE AND VIBRATION...10

2.1 Introduction.....10
2.2 Noise and Vibration issues.....11
2.3 PMSM Drive System.....11
2.4 Torque – speed characteristics of an ideal PMSM.....12
2.5 PMSM d-q Model.....13
2.6 Noise and Vibration in PMSM.....16
2.6.1 Electromagnetic.....16
2.6.2 Mechanical.....17
2.6.3 Aerodynamic.....18
2.7 Conclusion.....19

CHAPTER 3: IMPROVING TORQUE RIPPLE, NOISE AND VIBRATION.....20

3.1 Introduction.....20
3.2 Reduction methods.....20
3.2.1 Design Based Methods.....20
a.) Cogging torque.....21
b.) Torque ripple.....24
3.2.2 Control Based Methods.....28
3.3 Conclusion.....29

CHAPTER 4: DESIGN METHODOLOGY FOR PMSM……31

4.1 Introduction……31
4.2 Design Methodology……31
4.3 Design steps……33
4.3.1 Design Ratios……35
4.3.2 Envelope Sizing……35
4.3.3 Rotor Torque density……35
4.3.4 Stator and Rotor Sizing……36
4.3.5 Computation of Maximum Number of Turns in the Slot……37
4.3.6 Number of Phases and Slot/Pole Combinations……37
4.4 Measurement for Torque pulsations……39
4.4.1 Electrical measurements……39
4.4.2 Mechanical Measurements……40
4.4.3 Simulation and analysis……40
4.5 Motor design……41
4.6 Design of controller……42
4.7 Soft computing design……44
4.8 Conclusion……45

CHAPTER 5: REDUCTION TECHNIQUES……46
5.1 Introduction……46
5.2 Cogging Torque and Torque Ripple Reduction of IPSM Using Asymmetric Flux Barriers……47
5.2.1 Analysis of Torque Performance……47
5.2.2 Analysis of reluctance torque ripple……50
5.3 Unequal Teeth Widths for Torque Ripple Reduction in Permanent Magnet Synchronous Machines with Fractional-Slot Non-Overlapping Windings……51
5.4 Cogging Torque Minimization and Torque Ripple Suppression in Surface-Mounted Permanent Magnet Synchronous Machines Using Different Magnet Widths……56
5.5 Torque Ripple Reduction of Axial Flux Permanent Magnet Synchronous Machine with Segmented and Laminated Stator……58
5.5.1 Axial flux permanent magnet synchronous machine with segmented and laminated stator……59
5.5.2 Torque ripple assessment using an analytical approaches……59

Conclusion……63

Bibliography……64

LIST OF FIGURES

1.1 History of PM materials.....4
1.2 Interior permanent magnet synchronous motor.....4
1.3 Surface mounted, Embedded and Interior permanent magnet synchronous motors.....5

2.1 Torque fluctuation components in the electromagnetic torque of the PMSMs.....10
2.2 PMSM motor drive system.....12
2.3 Torque/speed and power/speed characteristics of an ideal PMSM.....13
2.4 PM machine synchronously rotating d-q reference frame.....15
2.5 Typical relative contributions to total sound power radiation as function of speed.....18

3.1- Slot openings spread over the surface area.....22
3.2-Teeth pairing in stator slot and corresponding permeance function.....23
3.3- Defining magnet parameters, pole arc angle, and pole pitch.....26

4.1- Air gap flux distribution pattern for cases when pole pitch and slot pitch are equal and different.....32
4.2- Flowchart of the overall design methodology of PMSM.....34

5.1 Parameters of flux-barriers to be optimized.....47
5.2 a.) Electromagnetic torque under full-load condition in CCW direction.....49
5.2 b.) Electromagnetic torque under full-load condition in CW direction.....49
5.2 C.) Cogging torque under no-load condition in CCW direction.....49
5.2 d.) Cogging torque under no-load condition in CW direction.....49
5.3 Reluctance torque under full-load condition in CCW direction.....50
5.4 Flux densities in the stator teeth of the original 12-slot 10-pole PMSM (with equal teeth widths) and of the redesigned PMSM (with unequal teeth widths) at the nominal load.....52
5.5 a) Torque curves of the skewed and non-skewed original 12-slot 10-pole PMSM (with equal teeth widths) and of the redesigned PMSM (with unequal teeth widths) at the nominal load.....53
5.5 (b) Spectrum analysis of the torque curves.....53
5.6 a) Cogging torque curves of the skewed and non-skewed original 12-slot 10-pole PMSM (with equal teeth widths) and of the redesigned PMSM (with unequal teeth widths) at no-load.....54
5.6 (b) Spectrum analysis of the torque curves.....54

5.7 Cross section of rotor of surface mounted PMSM. (a) Uniform magnet rotor. (b) Different magnet widths method……56
5.8 Peak cogging torque of three representative PMSMs with different which is calculated by FEA……57
5.9 Rotor magnet optimization and arrangements……61
5.10 Peak-to-peak values of cogging torque for different magnet shapes……..62

LIST OF TABLES

2.1 Motor parameters & variables……16
5.1 Optimal values of flux-barrier parameters……48
5.2 Comparison of average torque and torque ripple under different conditions……48
5.3 Key design parameters of the proposed machine……60

List of Symbols

B	flux density	[T]
B_δ	fundamental open-circuit airgap flux density	[T]
B_n	radial component of the airgap flux density	[T]
B_t	tangential component of the airgap flux density	[T]
B_m	peak value of the flux density	*[T]*
B_r	remanence flux density of the PM	*[T]*
d	denominator of q	-
D	inner stator diameter	[m]
E	induced voltage	[V]
E_i	EMF phasor of conductor I	[V]
E_0	fundamental back-EMF	[V]
E_{magn}	stored magnetic energy	[J]
E_n	*nth* harmonic component of the phase back-EMF	[V]
f	frequency	[Hz]
H_m	coercive magnetic field intensity of the PM	[A/m]
i	*phase current*	[A]
i_f	current in a winding modelling the PM	[A]
I	amplitude of the current	[A]
I_{ch}	characteristic current	[A]
I_r	rated current	[A]
I_d	d-axis current	*[A]*
I_q	q-axis current	*[A]*
k	integer 1, 2, 3...	-
k_C	carter factor	-
k_h	hysteresis coefficient	[W.s/T^2/m^3]
k_e	coefficient of excess loss	[W.(s/T)$^{3/2}$/m^3]
k_f	stacking factor	-
k_{wn}	*nth* harmonic component of winding factor	-
L	active length	[m]
L	inductance	[H]

L_a	self-inductance of phase a	[H]
L_d	*d*-axis inductance	[H]
l_m	PM thickness	[m]
M	mutual inductance varying with θ	[H]
m	number of phases	-
n	rotational speed	[rpm]
n	integer 1, 2, 3...	-
n_l	number of layers of the winding	-
n_u	numerator of q	-
p	number of poles	-
P_{in}	input power	[W]
P_{out}	output power	[W]
P_{cu}	copper losses	[W]
P_{iron}	iron losses	[W]
q	number of slots per pole per phase	-
Q	reactive power	[VAR]
Q_s	number of stator slots	-
R	resistance of one phase of the stator winding	[Ω]
S	vector describing a sequence of conductors of phase A	-
S_1	fundamental current loading	[A/m]
t	time	[s]
T	torque	[Nm]
T_{cog}	cogging torque	[Nm]
T_{loss}	“loss” torque	[Nm]
T_{mean}	mean value of the torque	[Nm]
T_{rip}	torque ripple	[p.u.]
U	voltage	[V]
V	supplied phase voltage	*[V]*
v	Volume	[m^3]
W	magnetic energy	[J]
w_m	PM length	[m]
X	machine periodicity	-

Greek Symbols

α	magnet angle	[rad]
β	angle between the *d*-axis and the current vector	[rad]
δ	airgap length	[mm]
δ	load angle	[rad]
γ	angle between the line current and back-EMF	[rad]
μ_0	magnetic permeability of free space	[H/m]
μ_r	relative magnet permeability	-
φ	angle between phase current and phase voltage	[rad]
Ψ_a	flux seen by phase a	[Wb]
ψ_m	magnet flux linkage	[Wb]
σ	material conductivity	[Ωm^{-1}]
σ	radial magnetic force density	[N/m^2]
Θ	angular position	[rad]
ω	electrical angular frequency	[Hz]
Ω	rotor speed	[rad/s]

ABSTRACT

This book deals with the Permanent magnet synchronous machines, paying particular attention to the analysis of cogging torque and torque ripple of the machine. Permanent magnet synchronous machines are vulnerable to significant amounts of torque ripple if they are not carefully designed. Torque ripple is the parasitic element that causes mechanical vibration, acoustic noise and even latent operational failure in permanent magnet (PM) machines. Consequently, considerable design efforts should be made to minimize torque ripple of the machines for high performance applications. Even though minimizing cogging torque can help reduce the torque ripple, but cannot definitely give rise to a low level torque ripple. In order to accurately analyze the torque ripple of the machine and make it possible to reduce the cogging torque under load condition, it is necessary to calculate the cogging torque accurately. Therefore some calculation methods which supports the analysis of cogging torque and torque ripple of the machine is also proposed in this study. Different methods are also explained for the mitigation of cogging torque and torque ripple and design of a machine with reduced toque ripples.

ASTRATTO

Questo libro tratta le macchine sincrone a magneti permanenti, pagando in particolare attenzione all'analisi della coppia di intasamento e dell'ondulazione della coppia della macchina. Le macchine sincrone a magneti permanenti sono vulnerabili a quantità significative di ondulazione di coppia se non sono progettate con cura. L'increspatura della coppia è l'elemento parassitario che causa vibrazioni meccaniche, rumore acustico e persino guasti operativi latenti nelle macchine a magneti permanenti (PM). Di conseguenza, è necessario compiere notevoli sforzi di progettazione per ridurre al minimo l'ondulazione di coppia delle macchine per applicazioni ad alte prestazioni. Anche se ridurre al minimo la coppia di cogging può aiutare a ridurre l'ondulazione di coppia, ma non può sicuramente dare origine a un'ondulazione di coppia di basso livello. Al fine di analizzare accuratamente l'ondulazione di coppia della macchina e consentire di ridurre la coppia di cogging in condizioni di carico, è necessario calcolare accuratamente la coppia di cogging. Pertanto, in questo studio vengono proposti anche alcuni metodi di calcolo che supportano l'analisi della coppia di intasamento e dell'ondulazione della coppia della macchina. Vengono inoltre spiegati diversi metodi per la mitigazione della coppia di intasamento e dell'ondulazione della coppia e la progettazione di una macchina con increspature ridotte.

CHAPTER 1

PERMANENT MAGNET SYNCHRONOUS MACHINES

1.1 Introduction

Electric energy forms the backbone of modern civilization. Efficient energy consumption is the key to solving the 21st century global issues on climate change. Electric motors consume over 65% of the world's generated electrical power, and hence improvements in the efficiency of motors make significant imprints on reduction of its consumption. The evolution of PM motors began in the early 1940s when the hysteresis motor was introduced by Teare. The insertion of PMs into the rotor bridge of a double-cage induction motor was reported by Alger in the 1950s. The hysteresis motor was the forerunner of the modern IPM motors. A close examination reveals that different technological advancements and market forces have combined sometimes in fortuitous ways to accelerate the development of high-efficiency interior permanent magnet (IPM) synchronous motors.

The history of the development of the IPM motors is linked to the advancement of high-energy PM materials over the past 100 years. Figure 1.1 timelines the brief history of the development of hard PM materials. [1]

1.2 Construction of Permanent magnet Synchronous machines

Permanent magnet synchronous machines generally have same operating and performance characteristics as synchronous machines. A permanent magnet machine can have a configuration almost identical to that of the conventional synchronous machines with absence of slip rings and a field winding. Fig.1.2 shows a cross section of simple permanent magnet synchronous machines. It consists of the stationary member of the machine called stator. Stator laminations for axial air gap machines are often formed by winding continuous strips of soft steel. Various parts of the laminations are the teeth slots which contain the armature windings. Yoke completes the magnetic path. Lamination thickness depends upon the frequency of the armature source voltage and cost. The working principle of permanent magnet synchronous motor is same as that of synchronous motor. When three phase winding of stator is energized from 3 phase supply, rotating magnetic field is set up in the air gap. At synchronous speed, the rotor field poles locks with the rotating magnetic field to produce torque and hence rotor continues to rotate.

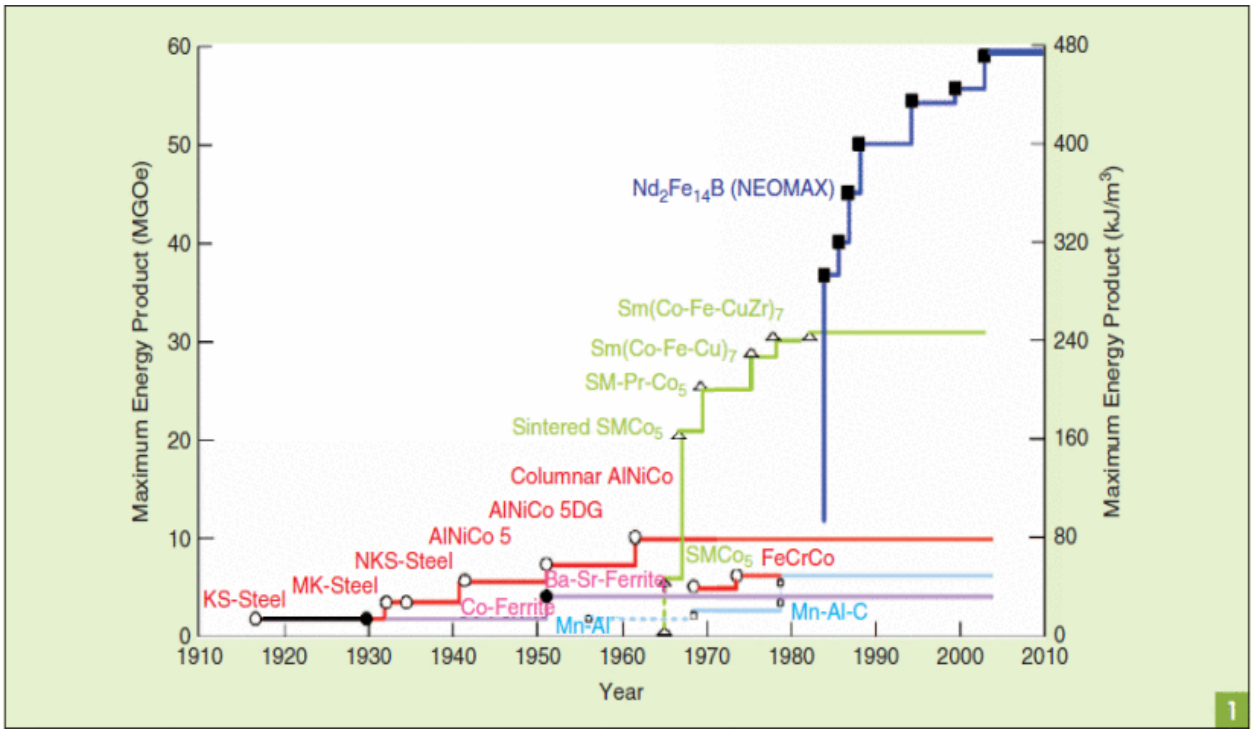

Fig 1.1 History of PM material

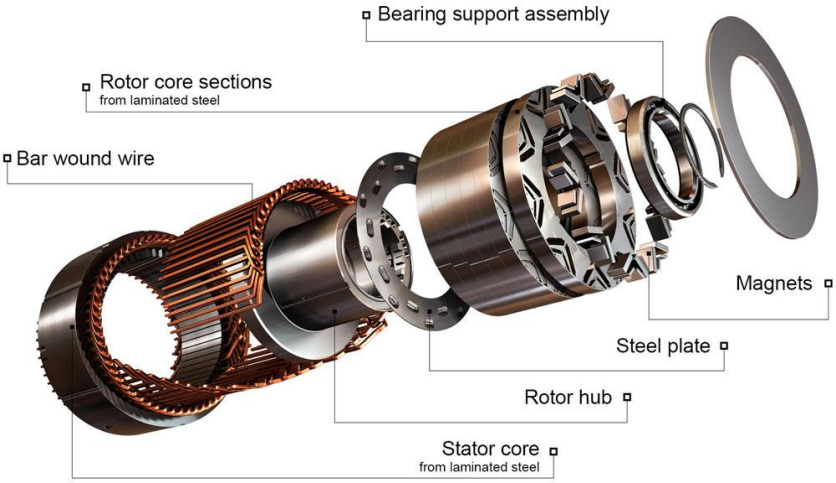

Fig 1.2 Interior permanent magnet synchronous motor

A permanent magnet synchronous motor, like any rotating electric motor, consists of a rotor and a stator. The stator is the fixed part. The rotor is the rotating part. Typically, the rotor is located inside the stator of the electric motor, there are also structures with an external rotor - inside out electric motors. The rotor consists of permanent magnets. Materials with high coercive force are used as permanent magnets.

According to the rotor design, synchronous motors are divided into:

- electric motors with salient pole rotor
- electric motors with non-salient pole rotor

An electric motor with non-salient pole rotor has an equal direct and quadrature inductances $L_d = L_q$, whereas for an electric motor with salient pole rotor the quadrature inductance is not equal to the direct $L_q \neq L_d$.[2]

Also, according to the design of the rotor, the PMSM are divided into:

- surface permanent magnet synchronous motor
- interior permanent magnet synchronous motor

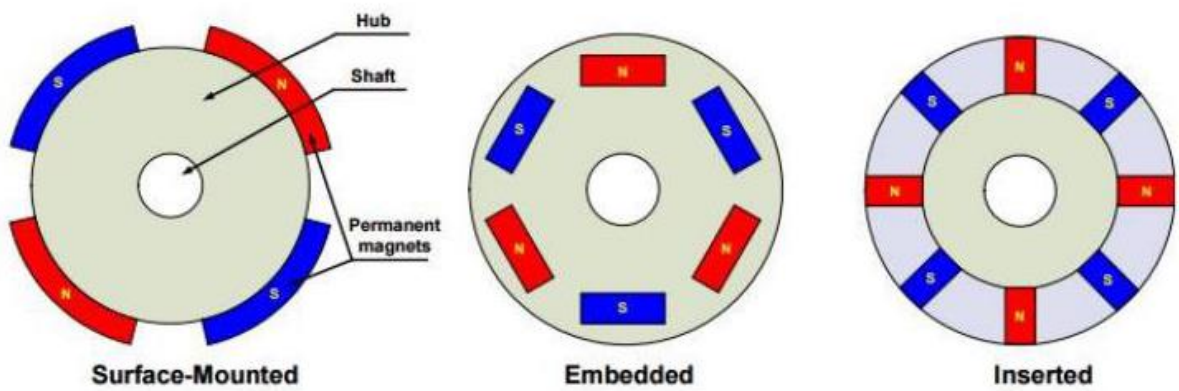

Fig 1.3 Surface mounted, Embedded and Interior permanent magnet synchronous motors

All electric motors function through the interaction between the magnetic field of the stator and the magnetic field of the rotor. How those magnetic fields are produced depends upon the motor design. Motors with permanent magnets include: DC permanent magnet, where the PM is the stator field, and DC current is applied to the rotor through brushes and a commutator; Brushless DC where the permanent magnets are installed on the rotor, and what is essentially an inverter feeds windings in the stator; and permanent magnet synchronous.

In an induction motor, an AC power supply is connected to windings in the stator. The rotor is essentially one large loop of conductor, called a squirrel-cage, built around a laminated iron core. The AC power causes a rotating magnetic field in the interior of the stator, which then cuts through the rotor conductors and induces a current in them. The current in the rotor then produces its own magnetic field, and the interaction between the rotor field and the stator field produces torque. If there is no speed difference between the rotor and the magnetic field of the stator, then no lines of magnetic flux are cut, no current is induced, and no magnetic field is generated in the rotor - thus, no torque. So, in the order for an induction motor to produce torque, there must be some

difference between the speed of the rotating stator field and the speed of the rotor. This difference is termed "slip."

In a permanent magnet machines the air gap serves a role in that its length largely determines the operating point of the permanent magnet in the no-load operating condition of the machines. Also, longer air gaps reduce machines windage losses. Many permanent magnet synchronous machines may be cylindrical or smooth rotor physically but electrically the magnet is still equivalent to a salient pole structure. Some of the PMSM rotors have the permanent magnets directly facing the air gap. Rotor yoke is the magnetic portion of the rotor to provide a return path for the permanent magnets also provide structural support. The yoke is often a part of the pole structure A synchronous machine is just an electromechanical transducer which converts mechanical energy into electrical energy or vice versa. The fundamental phenomenon or law which makes these conversions possible are known as the Law of Electromagnetic Induction and Law of interaction.

- Law of Electro-Magnetic Induction

This law is also called as Faraday's First Law of Electromagnetic Induction. This law relates to the production of emf, i.e; emf is induced in a conductor whenever it cuts across the magnetic field.

- Law of Interaction

This law relates to the production of force or torque, i.e., Whenever a current carrying conductor is placed in the magnetic field, by the interaction of the magnetic field produced by the current carrying conductor and the main field, force is exerted on the conductor producing torque..

1.3 Working of PM Synchronous machines

The PMSM has a stator with a set of 3-phase sinusoidally distributed copper windings and a rotor with permanent magnets. A sinusoidal magnetic field is generated in the air gap when 3-phase balanced sinusoidal currents are supplied in the 3-phase stator windings. The rotor magnetic field produced by the permanent magnets can be made sinusoidal by shaping the magnets and controlling their magnetizing directions. The electromagnetic torque is generated on the shaft by the interaction of these two magnetic fields created by the stator and the rotor circuits. In the surface mounted PMSM, the magnets are epoxy-glued or wedge-fixed to the cylindrical rotor. The manufacturing of this kind of a rotor is simple. However, the strength of the rotor is only as good as that of the epoxy glue. The d- and q axes inductances of the surface mounted PMSM are approximately

equal. This is because the length of the air gap is equal to that of the magnet, which has a permeability that is approximately the same as that of the air.

In the inset PMSM, the magnets are put into the rotor surface slots that secure the magnet in its location. Interior PMSM has its magnets buried inside the rotor, which is even more secure. The manufacturing process is complicated that makes the interior PMSM more expensive compared to the other PMSMs. The interior PMSMs can stand small amount of demagnetizing current; this makes the motor suitable for field weakening operation in the high-speed range. The q- axis inductance can be much larger than that of the d-axis although the length of the air gap is the same. The space occupied by the magnet in the d-axis is occupied by iron in the q-axis. This means that in addition to the electromagnetic torque (also known as mutual torque), a reluctance torque exists in interior and inset PMSMs.

The working principle of permanent magnet synchronous motor is same as that of synchronous motor. When three phase winding of stator is energized from 3 phase supply, rotating magnetic field is set up in the air gap. At synchronous speed, the rotor field poles locks with the rotating magnetic field to produce torque and hence rotor continues to rotate. As we know that synchronous motors are not self-starting, PMSM needs to be started somehow. A permanent-magnet synchronous motor (PMSM) uses permanent magnets embedded in the steel rotor to create a constant magnetic field. The stator carries windings connected to an AC supply to produce a rotating magnetic field. At synchronous speed, the rotor poles lock to the rotating magnetic field.

The operation of a synchronous motor is due to the interaction of the magnetic fields of the stator and the rotor. Its stator winding, which consists of a 3phase winding, is provided with a 3phase supply, and the rotor is provided with a DC supply. The 3phase stator winding carrying 3 phase currents produces 3 phase rotating magnetic flux (and therefore a rotating magnetic field). The rotor locks in with the rotating magnetic field and rotates along with it. Once the rotor field locks in with the rotating magnetic field, the motor is said to be in synchronization. A single-phase (or two-phase derived from single phase) stator winding is possible, but in this case the direction of rotation is not defined and the machine may start in either direction unless prevented from doing so by the starting arrangements.

Once the motor is in operation, the speed of the motor is dependent only on the supply frequency. When the motor load is increased beyond the breakdown load, the motor falls out of synchronization and the field winding no longer follows the rotating magnetic field. Since the motor cannot produce (synchronous) torque if it falls out of synchronization, practical synchronous motors have a partial or complete squirrel-cage damper winding to stabilize operation and facilitate starting. Because this winding is smaller than that of an

equivalent induction motor and can overheat on long operation, and because large slip-frequency voltages are induced in the rotor excitation winding, synchronous motor protection devices sense this condition and interrupt the power supply (out of step protection). PMSM provides rotation at a fixed speed in synchronization with the frequency of the power source. PMSMs are therefore ideal for high-accuracy fixed-speed drives. Boasting very high power density, very high efficiency and high response, the motor is suitable for most sophisticated applications in the industrial segment. It also has a high overload capability. A PMSM is largely maintenance free, which ensures the most efficient operation.[3]

1.4 Applications of PMSMs

PM motors are used in a broad power range of applications from a few mWs to hundreds of kWs. There are also attempts to use PMSMs for high power applications even for those rated over a MW. Thus, PM motors span a wide variety of application fields, from stepper motors for wristwatches through industrial drives for machine tools to large PM synchronous motors for ship propulsion.

In aerospace applications, the PM alternators are in competition with several other brushless synchronous machines, namely the inductor, Lundell, rotating rectifier, and various reluctance configurations. The PM BLDCs are also popular in the computer industry for reduced noise levels, the ability of precise speed and torque control, and flexibility of shape and geometry.

The largest users of PM machines today are by far the automotive industry; PMSMs seem to be the best propulsion motors for electric and hybrid road vehicles. It can be noted that, one rotating machine in passenger cars that is not PM-excited is the alternator. However, PM alternators are used in other automotive applications such as auxiliary power supplies in trucks and off-road vehicles.

The servo types of PM motors are used as variable-speed drives in applications where compact design, high efficiency, high power factor, and low noise are the primary requirements. Possible applications of these motors are in electro-hydraulic and/or electric brakes, power steering, and certain types of valve controls. Low torque ripple levels are required for these applications, since the motors have to work at low speeds with high precision in speed control.

1.5 Advantages of permanent magnet synchronous motor

- Heat generated in stator is easy to remove.
- High torque per frame size.
- Reliability due to absence of brushes and commutator.
- Highest efficiency.
- Synchronous operation makes field orientation easy.
- Good high-speed performance.
- Precise speed monitoring and regulation possible.
- Smooth torque.

1.6 Drawbacks of permanent magnet synchronous motor

- Rotor position sensing required.
- Position sensor or sensorless technique is required for motor operation.
- Difficult to startup the motor using sensorless technique.

1.7 Conclusion

Permanent magnet motors are more efficient than induction motor or motors with field windings for certain high-efficiency applications such as electric vehicles. Tesla's Chief Motor Designer was quoted discussing these advantages, saying: It's well known that permanent magnet machines have the benefit of pre-excitation from the magnets, and therefore you have some efficiency benefit for that. Induction machines have perfect flux regulation and therefore you can optimize your efficiency. Both make sense for variable-speed drive single-gear transmission as the drive units of the cars. So, as you know, our Model 3 has a permanent magnet machine now. This is because for the specification of the performance and efficiency, the permanent magnet machine better solved our cost minimization function, and it was optimal for the range and performance target. Quantitatively, the difference is what drives the future of the machine, and it's a trade-off between motor cost, range and battery cost that is determining which technology will be used in the future.[4]

Permanent magnet motors rely on neodymium. “Rare earth production is as bad as you can get in terms of environmental damage,” according to a trader in rare earth metals. China, the top producer of neodymium, restricted shipments to Japan in 2010 during a controversy over disputed ownership of islands. China imposed strict export quotas on several rare earth metals, saying it wanted to control pollution and preserve resources. The quotas were lifted in 2015. Although neodymium is relatively abundant, global demand for neodymium outstripped production by about 10% in 2017.

CHAPTER 2

PMSM ANALYSIS OF TORQUE RIPPLE, NOISE AND VIBRATION

2.1 Introduction

The goal in this chapter is to familiarize the readers with the torque ripple, noise and vibration in PMSMs. The origins of those issues and their minimization techniques from design perspective will be addressed. An extended literature review on the torque ripple and cogging torque as well as magnetic stress due to periodic excitation forces will also be presented.

Permanent magnet synchronous motors (PMSM) generally are classified into Interior permanent magnet synchronous motors (IPMSM) and the Surface permanent magnet synchronous motors (SPMSM). Regarding to the electromagnetic torque capability, the PMSMs generate torque only from the permanent magnets, however for the IPMSMs, the electromagnetic torque consists of two components, permanent magnet torque and the reluctance torque. One of the main problems presented by PMSM is the electromagnetic torque fluctuation being the cause of vibration, noise, speed variation and problems in control devices. Depending on the machine type, the main torque fluctuation components of the PMSMs are the cogging torque and torque ripples.[5]

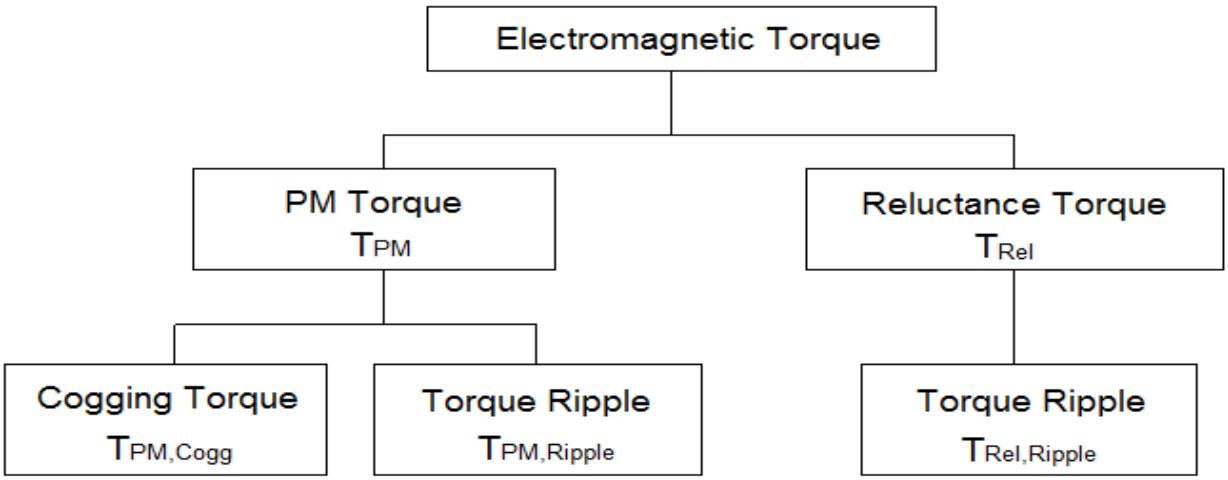

Fig 2.1Torque fluctuation components in the electromagnetic torque of the PMSMs.

Undesirable qualities such as cogging torque, torque ripple and unbalanced magnetic force (UMF) are parasitic effects which reduce not just the output torque but the life span of a given electric machine; in addition, it causes noise and vibration in the system.

2.2 Noise and Vibration issues

Vibration is a limited reciprocating particle motion of an elastic body or medium in alternately opposite directions from its equilibrium position when that equilibrium has been disturbed. In order to vibrate, the body or system must have two characteristics: elasticity and mass. The amplitude of vibration is the maximum displacement of a vibrating particle or body from its position of rest.
Sound is defined as vibrations transmitted through an elastic solid, liquid, or gas; sound waves with frequencies in the approximate range of 20 to 20,000 Hz are capable of being detected by human ears. Noise is disagreeable or unwanted sound. Distinction can be made between airborne noise and the noise traveling through solid objects. Airborne noise is the noise caused by the movement of large volumes of air and the use of high pressure. Structure-borne noise is the noise carried by means of vibrations of solid objects. The frequency of interest for vibrations is generally within 1000 Hz, and for noise it is over 1000 Hz.

The acoustic noise in electric motors based on its source can be classified into three categories: aerodynamic, mechanical, and electromagnetic. The aerodynamic noise consists of windage noise due to air turbulence around the rotor and the noise from blowers used for ventilation. Most of the mechanical noise is associated with the bearing assembly of a motor; they may be significant if, for example, the bearing parts are deformed in some manner, or if excessive clearances permit axial travel of the shaft. In addition, inertia forces caused by an unbalanced rotor known as eccentricity can cause mechanical noise. Electromagnetic noise is often the dominant type of noise in modern small motors. Several design related factors like slotting, saturation, eccentricities of shaft, rotor slots, spigots etc. can generate periodic electromagnetic exciting forces within the motor. These exciting forces act on the machine, which is seen as a mechanically passive system capable of vibrating and generate the vibratory motion.

The noise produced from any or all the three sources give rise to measurable deformations and vibrations. Part of the energy of the vibration motion within the audible range transforms into sound energy, depending on motor frame's sound radiation capacity. This sound energy is heard as acoustic noise [18]. The three noise production mechanisms will be discussed further in section.

2.3 PMSM Drive System

The phase windings of a PMSM are fed with sinusoidal waveforms shifted by $(360/Nph)^o$ from one another, where N_{ph} is the number of stator phases. For a three-phase machine, the three-phase windings with 1200 space phase shifted are fed by 120° time phase

shifted currents to produce a rotating magnetic field. This type of machine is called a sinewave motor.

The motor drive structure includes the machine, associated position sensors (if not sensor less operation), power electronics converter and the controller. A typical PMSM motor drive system is shown in Fig. 2.2. Generally, the feedback from the position sensor provides the rotor position information, which is used to appropriately energize the phase currents for machine operation in any of the torque, speed or position-controlled modes. Current sensors provide feedback to the controller to reconstruct the three phase currents for current control, which in turn allow torque control. The speed control, if necessary, is accomplished in the outer loop, and position-control, if necessary, is accomplished in yet another outer loop.

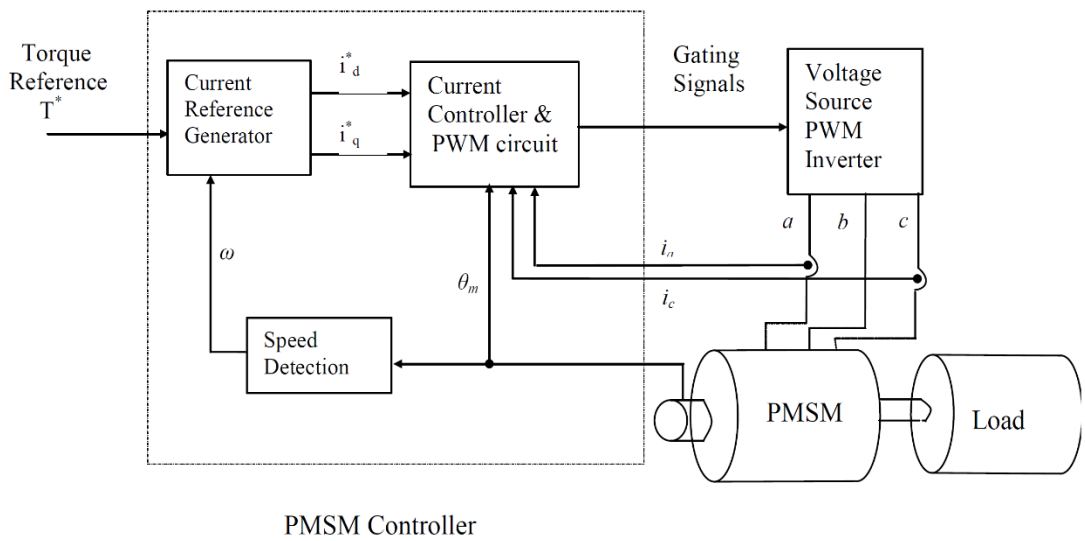

Fig 2.2 PMSM motor drive system

2.4 Torque – speed characteristics of an ideal PMSM

In a PMSM, the surface magnets are placed as alternate N and S poles. These magnets cause flux in the radial direction to flow through the air gap. Again, mmf generated due to the stator currents crosses the air gap and links the PM flux. The interaction of PM flux and stator mmf causes the rotor to rotate. As the rotor moves the flux linkage varies and induces BEMF in the stator phases. Finally, the interaction between the phase currents and the corresponding phase BEMFs produces the electromagnetic toque.
The stator phases in a PMSM are excited with sinusoidal currents; the phase BEMFs are desired to be sinusoidal through design. The speed variation can be achieved by varying the supply voltage, which is controlled by phase chopping or pulse width modulation

(PWM). The PMSM runs under torque limit mode until it reaches its continuous rated speed (also known as base speed or corner speed). This point gives the rated power output. Operating speeds above the base speed is generally obtained by phase advancing or field weakening. Field weakening is achieved by supplying negative reactive current. The motor operates under power limit mode with speeds higher than the base speed. The ideal torque/speed characteristic is plotted in Fig 2.3

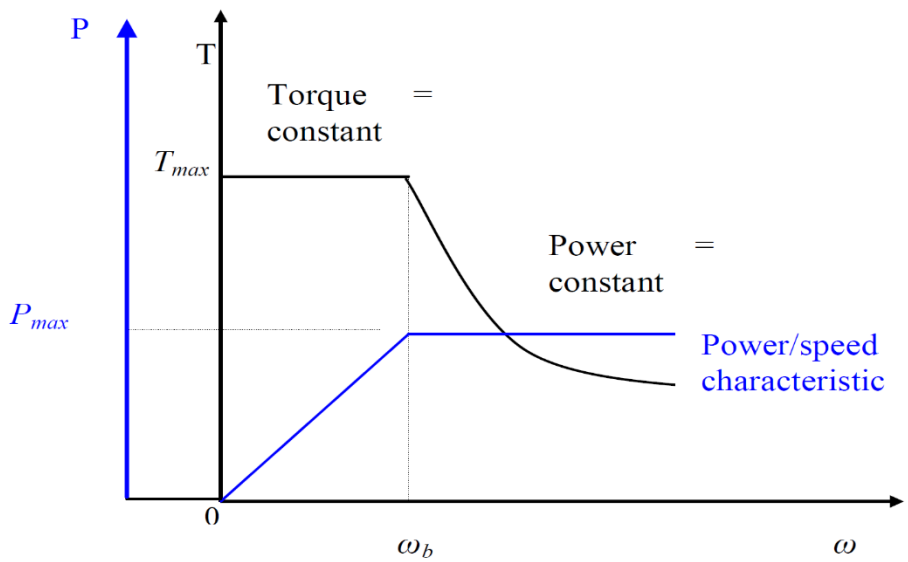

Fig 2.3- Torque/speed and power/speed characteristics of an ideal PMSM

The time variation of electromagnetic torque generated in a PMSM can be obtained as a product of stator currents and BEMFs. The fundamental components produce the continuous component of the torque, while harmonics of different frequency produce torque oscillations. In case of a sinusoidal distribution of currents and sinusoidal induced voltages, the electromagnetic torque is a constant quantity. The torque suffers from pulsating or AC components if either the BEMFs or the stator conductors' distribution is not purely sinusoidal. A qualitative representation of the torque waveform for sinusoidal phase currents and phase BEMFs containing a 5th order harmonics. Similar torque pulsations will be seen with harmonics in stator currents or with harmonics in both BEMFs and stator currents.

2.5 PMSM d-q Model

The electromagnetic analysis of a PMSM is conveniently carried out in a d-q rotating reference frame. The d-q reference frame variables are obtained from the stationary abc reference frame through the Park transformation equation given in (2.1). The Park transformation is a matrix transformation which converts a three phase balanced system into a two-dimensional. Two possible transformations are commonly used. The first one is α-β and is aligned with the "a" phase axis. It is called fixed reference frame. The other

case is usually called d-q rotor reference frame, which is aligned with the rotating magnetic axis of the rotor. The Park transformation converts the abc system to dq0 reference frame and dq0 system to abc reference frame. In the abc reference frame, three phase voltage, current or flux linkage quantities are represented by fa, fb and fc. The direct and quadrature axes equivalent voltages and currents are represented as fd and fq, respectively. The third component in the d-q frame is called "0" or homopolar component, which is identically zero in balanced three phase systems, and will be omitted later in this chapter. The transformation equations are

$$\begin{bmatrix} f_q \\ f_d \\ f_0 \end{bmatrix} = \frac{2}{3}\begin{bmatrix} \sin(\theta_r) & \sin(\theta_r - 2\pi/3) & \sin(\theta_r + 2\pi/3) \\ \cos(\theta_r) & \cos(\theta_r + 2\pi/3 & \cos(\theta_r + 2\pi/3) \\ 1/2 & 1/2 & 1/2 \end{bmatrix} . \begin{bmatrix} f_a \\ f_b \\ f_c \end{bmatrix}$$

……. (2.1)

$$\begin{bmatrix} f_a \\ f_b \\ f_c \end{bmatrix} = \begin{bmatrix} \sin(\theta_r) & \cos(\theta_r) & 1 \\ \sin(\theta_r - 2\pi/3) & \cos(\theta_r - 2\pi/3 & 1 \\ \sin(\theta_r + 2\pi/3) & \cos(\theta_r + 2\pi/3) & 1 \end{bmatrix} . \begin{bmatrix} f_q \\ f_d \\ f_0 \end{bmatrix}$$

The machine voltage equation in the abc reference frame can be expressed in matrix form as

$$\begin{bmatrix} v_a \\ v_b \\ v_c \end{bmatrix} = \begin{bmatrix} R_a & 0 & 0 \\ 0 & R_b & 0 \\ 0 & 0 & R_c \end{bmatrix} \begin{bmatrix} i_a \\ i_b \\ i_c \end{bmatrix} + \frac{d}{dt}\begin{bmatrix} \varphi_a \\ \varphi_b \\ \varphi_c \end{bmatrix}$$

……. (2.2)

where v_a, v_b, and vc are the machine phase voltages, referenced to the ground, i_a , i_b , and i_c are the machine phase currents, R_a , R_b , and R_c are the machine phase resistances, and ϕ_a , ϕ_b , and ϕ_c are the magnetic flux linkages associated with each phase. For the PMSM, the synchronously rotating d-q rotor reference is used. The abc and d-q reference frame directions are given in Fig. 2.4. The d-axis represents the rotor magnet flux axis and the q-axis is in quadrature to the d-axis.

The PMSM is represented by the standard dq mathematical model as [19]

$$v_d = Ri_d + L_d \frac{di_d}{dt} - pL_q \omega i_q$$

$$v_q = Ri_q + L_q \frac{di_q}{dt} + pL_d \omega i_d + k_t \omega$$

……. (2.3)

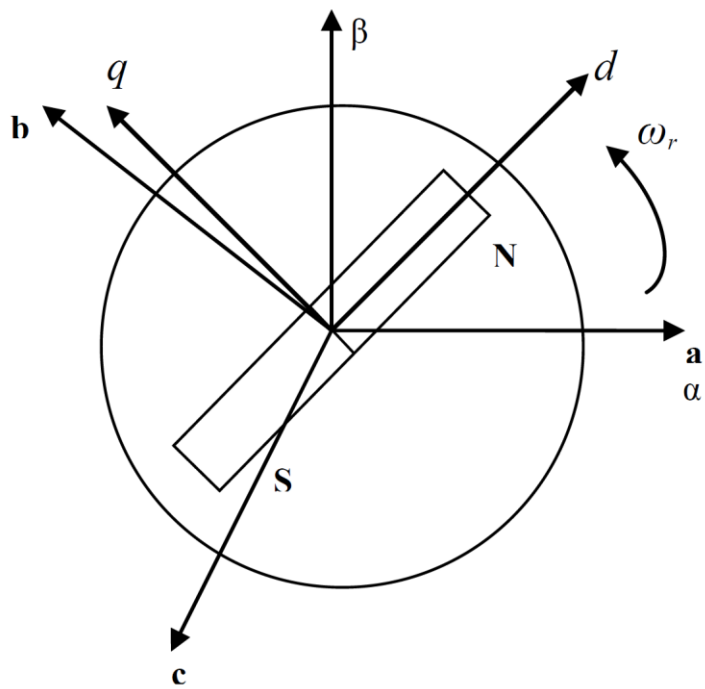

Fig 2.4- PM machine synchronously rotating d-q reference frame

The electromagnetic torque is

$$T_m = \tfrac{3}{2}(k_t i_q + p(L_d - L_q) i_q i_d) \qquad \text{..... (2.4)}$$

The motor dynamics are given by

$$T_m - T_{load} - T_{fr} = J\frac{d\omega}{dt} \qquad \text{..... (2.5)}$$

The stator phase voltage and currents are given by

$$v_s = \sqrt{v_d^2 + v_q^2}; \quad i_s = \sqrt{i_d^2 + i_q^2} \qquad \text{..... (2.6)}$$

The PMSM drive system model described by the above equations is valid for the ideal case without magnetic saturation. The parameters and variables of the model are listed in the Table 2.1.

v_q, i_q	q-axis stator voltage and current	v_d, i_d	d-axis stator voltage and current
R	Stator phase resistance	v_s, i_s	Stator phase voltage and phase current
L_q	Stator inductance in q axis	L_d	Stator inductance in d axis
k_t	Torque constant	p	Number pairs of poles
ω	Instantaneous rotational speed, $\omega>\Omega$	Ω	Rotational speed at a load-torque slope break point
T_m	Motor electromechanical torque	T_{load}	Load torque
T_{fr}	Friction torque	J	Moment of inertia

Table 2.1: Motor parameters & variables

2.6 Noise and Vibration in PMSM

It is very important to consider the noise and vibration problems during the process of electrical machine design. Electrical machine noise mainly consists of noise from electromagnetic, aerodynamic and mechanical origins. The machine vibration is primarily due to the eccentric position of the rotor with respect to the stator bore. The rotor eccentricity can be caused as a result of imperfection in rotor assembly which leads to shaft misalignment. Also, the unbalanced magnetic pull, if present in a motor even with perfectly aligned shaft, can create the rotor eccentricity. As a result, unbalanced forces exist in the machine air-gap that influences the radial vibration behavior, and therefore, the noise of the motor. The three categories of noise and vibration in electric machines are discussed below [20-22].

2.6.1 Electromagnetic

Electromagnetic (EM) vibration and noise are associated with parasitic effects due to higher space and time harmonics, eccentricity, phase unbalance, slot openings, magnetic saturation, and magnetostrictive expansion of the core laminations. The vibrating capability of the electronic machine is a function of two parameters, namely the mode number and the frequency. An annoying situation of “resonance’ arises where the frequency of the periodic exciting force is identical with or close to one of the natural frequencies of the machine. Electromagnetic (EM) vibration and noise are associated with parasitic effects due to higher space and time harmonics, eccentricity, phase unbalance, slot openings, magnetic saturation, and magnetostrictive expansion of the core laminations. The vibrating capability of the electronic machine is a function of two

parameters, namely the mode number and the frequency. An annoying situation of "resonance' arises where the frequency of the periodic exciting force is identical with or close to one of the natural frequencies of the machine.

Electromagnetic vibration and noise are caused by generation of electromagnetic fields. Both stator and rotor excite magnetic flux density waves in the air gap. If the stator produces magnetic flux density wave and rotor produces magnetic flux density wave, then the magnetic stress wave in the airgap is proportional to the product of the flux densities given as [23].

$$\frac{1}{2}\{B_{m1}B_{m2}\cos[(\omega_1+\omega_2)t+(k+l)\alpha+(\phi_1+\phi_2)] + B_{m1}B_{m2}\cos[(\omega_1-\omega_2)t+(k-l)\alpha+(\phi_1-\phi_2)]\} \quad \text{..... (2.7)}$$

where B_{m1} and B_{m2} are the amplitudes of the stator and rotor magnetic flux density waves, ω_1 and ω_2 are the angular frequencies of the stator and rotor magnetic fields, ϕ_1 and ϕ_2 are phases of the stator and rotor magnetic flux density waves, and k=1,2,3… and l = 1,2,3…

The magnetic stress wave in the airgap along with the slots, distribution of windings in slots, input current waveform distortion, air gap permeance fluctuations, and phase unbalance gives rise to mechanical deformations and vibrations. The electromagnetic excitation sources in a PMSM are cogging torque, mutual torque ripple, and radial attractive force fluctuation between the rotor and stator.

2.6.2 Mechanical

Mechanical vibration and noise is mainly due to bearings, their defects, journal ovality, sliding contacts, bent shaft, rotor unbalance, shaft misalignment or rotor eccentricity, couplings, U-joints, gears etc. The rotor should be precisely balanced as it can significantly reduce the vibration. The rotor unbalance causes rotor dynamic vibration and eccentricity, which in turn results in noise emission from the stator, rotor, and rotor support structure. Again, the rotor eccentricity causes unbalanced magnetic pull in the airgap that leads toward vibration. For simplicity, eccentricity is considered as a magnetic source for noise and vibration rather than a mechanical source. This research will ignore the vibration and noise coming from mechanical sources since the relative magnitude of noise from mechanical sources in medium to small power motors is small compared to EM sources.

With appropriate design and manufacturing quality controls, mechanical noise normally has less contribution to the overall noise level of small/medium sized motors than the other two sources.

2.6.3 Aerodynamic

The basic source of noise of aerodynamic nature is the fan. Any obstacle placed in the air stream produces noise. In unsealed motors, the noise of the internal fan is emitted by the vent holes. In totally enclosed motors, the noise of the external fan predominates. According to spectral distribution of the fan noise, there is a broadband noise (100 to 10,000 Hz) and siren noise (total noise). The siren effect is a pure tone being produced as a result of the interaction between fan blades, rotor slots, or rotor axial ventilation ducts and stationary obstacles. Increasing the distance between the impeller and the stationary obstacle can reduce siren noise. Small motors with shaft driven fans radiate much less noise when the speed is reduced below the rated speed. As the speed increases, the cooling fan becomes the primary source of noise. On the other hand, for motors with separately driven fans, no improvement in airflow noise is achieved when the speed is reduced. Through continuous development of material science, design, and manufacturing technology, modern motors have smaller loss and better heat dissipation than those of previous generations; this allows the use of a smaller fan for cooling. Also, fan blade design technology has also improved.

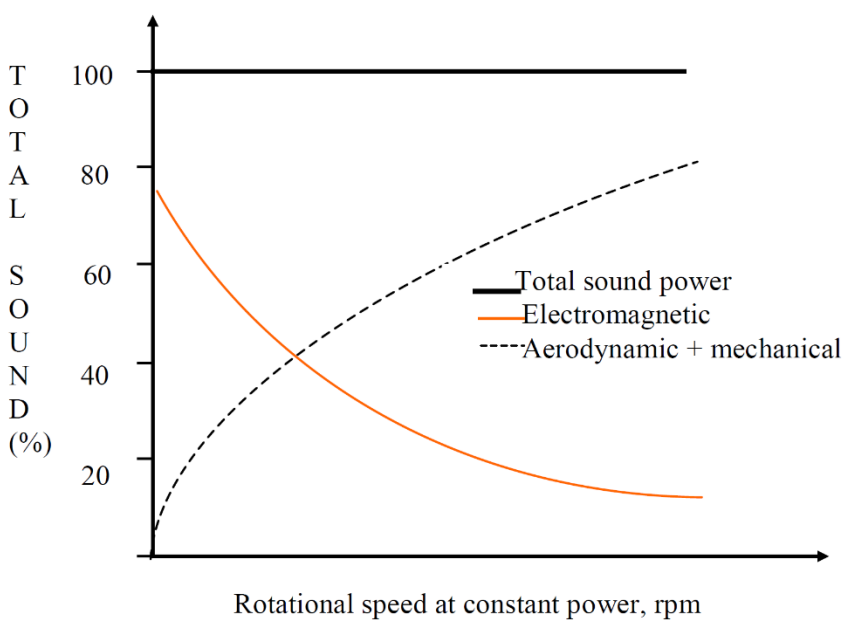

Fig 2.5- Typical relative contributions to total sound power radiation as function of speed

All these efforts minimize the motor aerodynamic noise. Large motors where the size of the cooling fan or blower is also large, the contribution of aerodynamic noise is significant. Small to medium size PMSMs with moderate speed has very little windage noise; the cooling fan, if any, does not contribute much to the total noise.

The contributions to the total noise by all three categories are shown in Fig. 2.5 [14]. The contribution of electromagnetic source dominates mechanical and aerodynamic causes especially in case of a medium to low power PMSM. The large power motor (around 1 MW range) uses cooling fan or blower that is the dominant cause of noise. Also, these motors when used for high-speed applications suffer from additional mechanical noise caused by rotor bearing, gear or friction.

2.7 Conclusion

Simple, low-cost, and effective ways to reduce torque ripple, noise and vibration in PMSM cannot be found in the literature. The literature also claims the indirect effect of cogging torque reduction in reducing the torque pulsations in [6, 11, and 17] without validation. The research presented in this dissertation will formulate a methodology to choose a design with rotor skewing that can minimize the torque ripple. It will also show the magnet design cases where torque ripple gets worse even after rotor skewing. This research will show how the different shapes of magnet for one particular-pole arc can make differences in the peak-to-peak torque ripple in a skewed motor compared to its non-skewed version. This research will also show in detail the stator excitation due to magnetic radial pressure, the mode shapes and mode frequencies responsible for structural vibration, and how this phenomenon varies with motor topology and winding configuration. In this regard, a detailed analytical model for predicting radial displacement as well as vibration based on radial pressure on the tooth will be included in this research.

CHAPTER 3

IMPROVING TORQUE RIPPLE, NOISE AND VIBRATION

3.1 Introduction

Low torque pulsations in motor drives are essential for high performance speed and position control applications where low acoustic noise and friendly human-machine interactions are demanded. The three torque components that contribute to torque ripples are reluctance torque, cogging torque and mutual torque. The reluctance torque in surface mounted PMSM is negligible; hence, it does not contribute to torque ripple. The cogging torque is a small fraction of total torque ripple. Thus, torque ripple improvement exclusively requires the reduction of key harmonics in BEMF and phase currents, which will minimize the mutual torque ripple component.

There is a fundamental relationship between noise and vibration in an electric machine. If the causes for the vibrating tendency of the electrical machine mechanical system can be eliminated or at least mitigated, then the noise and vibration will reduce considerably. The noise and vibration in the motors are mostly generated by the electromagnetic sources, which can subsequently be amplified by the dynamic characteristics of the motor structure. Certain factors of electromagnetic sources that give rise to measurable mechanical deformations and vibrations needs to be addressed properly to minimize the sound energy transformed from the vibrational energy.

3.2 Reduction methods

Noise and vibration reduction must start from the early design stages of the electric machine. This reduction method can be extended to some control-based techniques for further enhancing the quieter performance of the machine. Several techniques of both the methods from the existing literature are discussed in the following sections. There are two different approaches to accomplish such work; design-based approach and control based approach.

3.2.1 Design Based Methods

Rotor/stator skew, teeth pairing i.e., use of multiple teeth, choices of slot-pole combinations, use of slotted/non-slotted stator are the common design methods to improve cogging torque, torque ripple and magnetic stress waves in the airgap. The authors in [24,24, 26] proposed several design variations of improving cogging torque and showed how it minimizes the torque ripple of the machine. The work by S. Huang, M.

Aydin and T.A Lipo describes the appropriate selection of PM rotor shape and rotor skew angle to minimize the resultant sound power level, and hence, obtain a low noise motor design [10]. PM motors with fractional ratio of slot number to pole number have lower cogging torque but a considerable amount of unbalanced magnetic force [32]. Again slot-less motor has less torque ripple and zero cogging torque compared to slotted motor [10]. Different methods of design variations are discussed in the following section in the context of cogging torque improvement, torque ripple minimization and radial force reduction. A list of common measures in relation to design variation is given as follows elimination of slots [9,14,24,27,28,29,30,31]

- Skewed slots
- Special shape slot
- Selection of number of slots with respect to number of poles
- Decentered magnets
- Skewed magnets
- Shifted magnet segments
- Selection of magnet width
- Direction-dependent magnetization of PMs

Cogging torque:

The cogging torque is the consequence of the interaction between of the permanent magnets field and the stator slots, which produces reluctance variations with the rotor position, and it is independent of stator current. Cogging torque is the zero average pulsating torque caused by the tendency of the PM to align with the stator iron. This appears whenever magnet flux travels through varying reluctance. A simplified expression of cogging torque is given by equation (3.1) where ϕ_g is the magnet flux crossing the air gap and $\Re$ is the total reluctance through which the flux passes. Clearly, if the reluctance $\Re$ does not vary as the rotor rotates, the derivative in (2.1) is zero and the cogging torque is zero. In addition, cogging torque is independent of flux direction as the magnet flux ϕ_g is squared. Again, the reluctance of the PM and the iron core are negligible compared to air gap reluctance and thus the reluctance here exclusively refers to the air gap reluctance.

$$T_{cogg} = -\frac{1}{2}\phi_g^2 \frac{d\Re}{d\theta} \qquad \text{..... (3.1)}$$

Cogging torque results from interaction between the permanent magnets and the stator slots. The most common technique for cogging torque reduction is stator slot skewing. The idea is to reduce the change of reluctance with position and thus to reduce the cogging torque. The net change in reluctance can be minimized if the slot openings are spread over the surface area of the magnet as depicted in Fig. 3.1

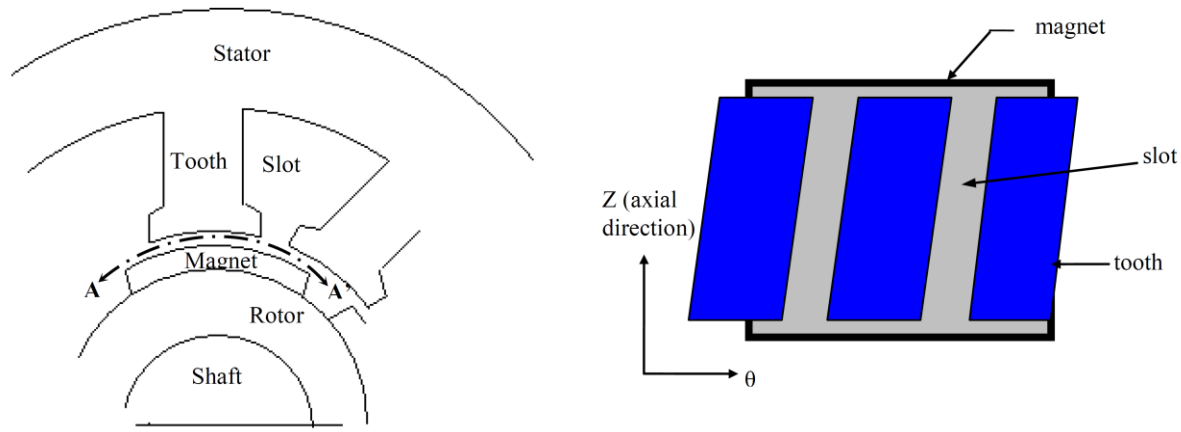

Fig 3.1- Slot openings spread over the surface area

Here, the slots are skewed so that each magnet sees a net reluctance that stays the same or nearly the same as slots pass by. In this way, changes along the axial dimension reduce the effect of changes along the circumferential dimension. As a result, the $d\Re/d\theta$ experienced by the entire magnet decreases, and consequently, the cogging torque decreases.

The same effect can also be obtained by shaping the stator slots using any of the following techniques:

a) Bifurcated slots
b) Empty or dummy slots
c) Closed slots
d) Teeth with different width of the active surface (teeth pairing)

The same results can be achieved by skewing the PMs where each magnet can be represented by number of straight rotor bar segments offset from each other by a fixed angle. This type of magnet skew is called step skew. There is another type of skew called continuous skew where each magnet pole is a skewed rotor bar. [6]

The number of periods of the cogging torque waveform N_{period} during a rotation of a slot pitch depends on the number of slots and poles. For a rotor with identical PM poles, equally spaced around the rotor, N_{period} is given by

$$N_{period} = \frac{N_p}{HCF\{N_s, N_p\}} \qquad \text{..... (3.2)}$$

where Ns and Np are the number of stator slots and rotor poles, respectively, and HCF(N_s, N_p) gives the highest common between N_s and N .
The mechanical angle corresponding to each period required to completely-eliminate the cogging torque is the optimum skew angle θ_{skew} given by

$$\theta_{skew} = \frac{2\pi}{N_{period} N_s} \qquad \text{..... (3.3)}$$

Equation (3.3) shows that the cogging torque is also a function of stator slots and rotor poles. The closer the number of slots is to the poles, the higher is the cogging torque period and the lower is its amplitude. The selection of slot-pole combination can thus reduce cogging torque significantly. The use of slot less stator is another novel way of eliminating cogging torque [16]. Since the PM field and stator teeth produce the cogging torque, a slot less motor can totally-eliminate the cogging torque. A slot less structure requires increased air gap, which in turn reduces the PM excitation field. To keep the same air gap magnetic flux density, the height of PMs must be increased. Slot less PMSMs therefore use more PM material than slotted motors. The research by Hwang et al. shows the use of teeth pairing with two different tooth widths for significant improvement in the cogging torque. The airgap permeance function is modified as the period is doubled with teeth pairing compared to single tooth situation. A model of teeth pairing with simplest airgap permeance function is shown. The fundamental component of air gap permeance GnNL as well as the cogging torque can be eliminated with appropriate combinations of two different tooth widths a and b as shown In Fig 3.2. Without teeth pairing (i.e., a = b), the period of airgap permeance is 2π/Ns and with teeth pairing the period is 4π/Ns.

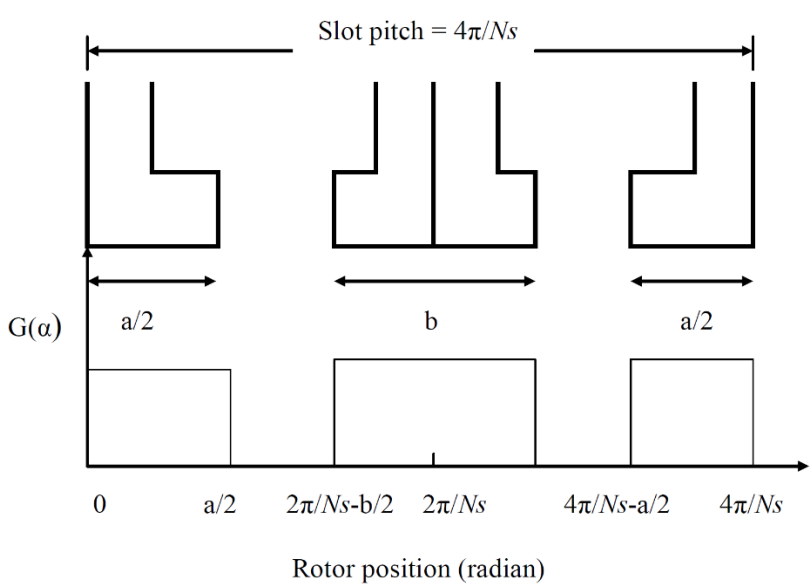

Fig 3.2-Teeth pairing in stator slot and corresponding permeance function

$$T_{cogg}(\theta) = -\frac{\partial W_g(\theta)}{\partial \theta} \propto \int_0^{2\pi} G^2(\alpha) B^2(\alpha,\theta) d\alpha \propto \sum_{n=0}^{\infty} nN_L G_{nN_L} B_{nN_L} \sin(nN_L\theta)$$

$$G_{nN_L} = \frac{N_s}{\pi}\frac{1}{nN_L} 2[\sin nN_L \frac{a}{2} + \sin nN_L \frac{b}{2}] \quad \text{.... (3.4)}$$

where NL is the least common multiple of Ns and Np, Wg and B are the air gap energy function and air gap flux density function, respectively.

Torque ripple

The PM torque ripple is the result of interaction of air-gap flux density high harmonics generated from the rotor magnets and stator winding. Reluctance torque ripple; For the salient rotor topologies, additional torque ripple components occur as results of interaction between the magnetic flux from stator currents and the rotor permeance harmonics. One of the main requirements during a new motor design for industry application is the low torque ripples and low cogging torque. For automobile application the torque ripple and cogging torque should be lower than 5% and 0.5% of the nominal torque, respectively. In several papers, numerous methods for reducing torque pulsations components, such as the magnet pole arc design, skewing of rotor magnets or stator slots, dummy slots, PM shifting, different slot width pairing etc.. The use of these techniques reduces the amplitude of torque pulsations, however they are related with additional drawbacks concerning the torque capability and production costs. Using the magnet pole arc design method, or dummy slots stator structure, increase the effective air-gap length that leads to the reduction of the air-gap flux density also the resulting effective torque. The skew of rotor magnets or stator slots is another effective method for reducing the both torque ripples and cogging torque components, and is widely using during the last time. For the PM machines, only step rotor skewing is possible when PMs are used: the rotor is split into two or more parts, each of them is skewed with respect to the others. Therefore, as results, the rotor skewing increases the production costs of the machine. On the other side, also the stator skewing is related with high production cost, but simultaneously, it additionally influences the stator winding length also the slot fill factor, and with this it increases the machine winding losses. Furthermore, depending on the skewed angle the both skew methods decrease the output torque of the machine.

Torque ripple can cause undesirable vibrations in the load response. Torque ripple consists of two components: electromagnetic torque fluctuation and cogging torque.

Electromagnetic torque ripple is caused by the harmonic interaction between the BEMF and the phase currents associated with the motor electrical dynamics.

The instantaneous electromagnetic torque for a 3-phase PMSM can be given by [7]

$$T_e = \sum_{x=a,b,c} \frac{e_x i_x}{\omega} + \frac{1}{2}\phi_g^2 \frac{d\Re}{d\theta} \qquad \text{..... (3.5)}$$

where ex and ix represent the phase BEMF and phase current, respectively, and the second term in the expression represents the cogging torque. The first term in (3.5) is known as the electromagnetic torque or the mutual torque. The motor can produce constant electromagnetic torque only if the part of the flux through stator windings due to the rotor field known as mutual flux is purely sinusoidal. This also requires sinusoidal spatial distribution of either the stator windings, or of the field due to rotor magnets. In practice, the perfect sinusoidal distribution is not achievable and the mutual flux contains higher harmonics and causes ripple in steady state torque in response to a purely sinusoidal current excitation. The torque ripple cannot be separated from cogging torque; most of the researchers mentioned these two issues together [11, 14 and 15]. Therefore, the design methods developed for reducing cogging torque can also be considered as the methods for reducing torque ripple.

Carlson et al. formulated an optimized design problem by evaluating the maximization of the EMF fundamental component and the minimization of the torque ripple without separating the different contributions [8]. The optimization problem was set as

min(f)
subject to $q_1 = 0$
$q_2 < 0$

where the cost function f is given by

$$f = \sum_{k=3,odd}^{\infty} c_{E,k} \frac{E_k^2}{E_1^2} - c_{E,1} \frac{E_1^2}{E_{1,\max}^2} + \sum_{k=1}^{\infty} c_{T,k} \frac{T_{c,k}^2}{T_0^2} \qquad \text{..... (3.6)}$$

Here, E_k^2 is the squared amplitude of the kth EMF harmonic component. $E_1^2$and $E_{1,max}^2$ are the squared amplitude of the first harmonic component and its maximum value (with pole arc equal to pole pitch), respectively.
The constraint $q_1 = 0$ guarantees the geometrical consistency of the rotor. In the constraint $q_2 < 0$, a lower bound to the distance between the magnets is taken. The unknowns of the optimization algorithm are the length of the magnets and their

positions, the skew length, and the number of tooth intervals r by which the pitch of the primary winding is shorted.

The first term of the optimization function minimizes the dominant BEMF harmonics of order 3, 5, 7 etc. to minimize ripple, the second term maximizes the fundamental harmonics to have maximum output torque, and the third term minimizes the cogging torque. Their analysis provided results showing the elimination of certain harmonics in BEMF for a particular value of magnet arc; this arc length depends on the number of poles in the machine, winding arrangement in the stator, and amount of magnet skew.

In surface mounted PM machines, the magnet shape determines the distribution of the air-gap magnetic field when influences of armature reactance of load currents are ignored. The practice is to start with a given magnet shape, and then to obtain the magnetic flux density curve by 2-D or 3-D FEA calculation. The curve is compared to the standard waveform and the FEA is repeated until a satisfactory waveform is obtained [9]. For example, if the 5th harmonic in BEMF needs to be eliminated then the pole arc angle (θm), shown in Fig. 3.3, should be selected such that 5 θm = n 1800, where n = 1,2,3,... If the machine has p pair of poles, then the mechanical degrees of θm is given as θm(mech) = θm/p. Generally, 5th and 7th order harmonics in BEMF are the most significant and any one of these can be eliminated completely by selecting the pole arc angle using the above procedure.

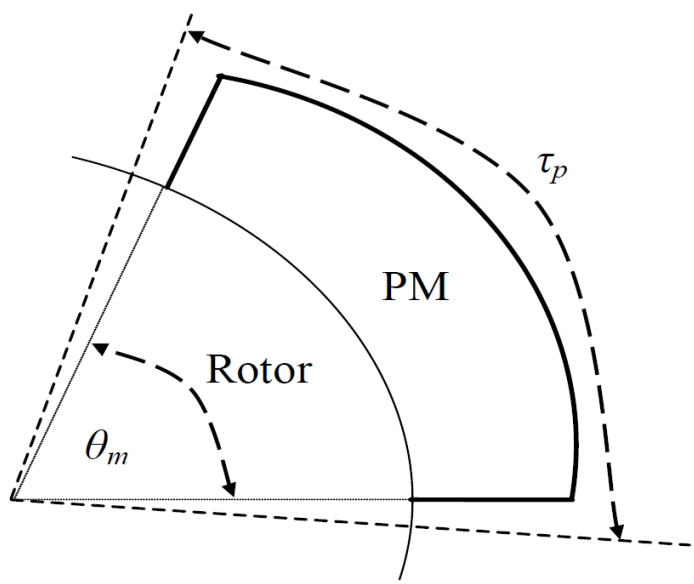

Fig 3.3- Defining magnet parameters, pole arc angle, and pole pitch

S. Huang, et al. in their research showed that the optimum selection of pole arc ratio and magnet skew angle can minimize the ripple torque and optimize the machine performance [10].

The sizing procedure starts by defining the output power as a product of air gap phase EMF and phase currents

$$P_e = \eta m \frac{1}{T} \int_0^T e(t) i(t) dt \qquad \text{..... (3.7)}$$

where e(t) and i(t) are the phase air gap EMF and phase current, respectively. These two periodic functions are given as

$$e(t) \propto NB_g \frac{f}{p} \lambda_0 D_0 L_{stk}$$

$$i(t) \propto \frac{A \pi \lambda_0 D_0}{(1 + K\phi)} \cdot \frac{1}{N} \qquad \text{..... (3.8}$$

The parameters used are:
η - machine efficiency
m - number of phases
T - period of the EMF
N - number of turns per phase
Bg - air gap flux density
f - converter frequency
p - pole pair
λ0 - ratio of outer surface diameter to air gap diameter
D0 - outer surface diameter
KΦ - ratio of electrical loading on rotor to stator
A - total electrical loading

The power output of the PMSM can be obtained by combining e(t) and i(t) in terms of the primary dimensions, magnet property, and electrical loading. The machine torque density and power density equations given by (3.8) can then be used to find the motor dimensions like outer surface diameter D0, rotor diameter to the airgap D_{tot}, and so on. These dimensions can be utilized to find the optimum values for magnet length and width.

$$T_{den} = \frac{P_e}{\omega \frac{\pi}{4} D_{tot}^2 L_{tot}}$$

$$P_{den} = \frac{P_e}{\frac{\pi}{4} D_{tot}^2 L_{tot}} \qquad \text{..... (3.9)}$$

The research presented in this dissertation investigate further to show that the variation in magnet shapes with the same pole arc ratio and skew angle can affect the torque ripple significantly. A systematic approach is then developed to design the PMSM with minimum torque ripple, and less noise and vibration.

3.2.2 Control Based Methods

Machine performances in terms of torque ripple, noise and vibration can also be improved by several control methods. Control techniques mainly use modulation of the stator current or BEMF waveforms. The control techniques adopted for obtaining ripple free torque and reduced radial forces are

- Open-loop control (harmonic cancellation technique) based on programme current waveform [32]
- Closed-loop control including flux and/or torque estimators [33]
- Alteration of motor commutation pattern, and therefore, the pattern of the force pulses [34]
- Increasing the number of stator phases to have lower radial forces [35]
- Concentrated windings with enlarged air gap for minimizing radial forces [34]
- Field weakening operation with higher currents for reduced radial forces in sinusoidally excited BLDC motors [36].

Bojan Grcar et al. proposed control-based reduction of pulsating torque for PMSMs [33]. The researchers subdivided the method into two basic groups: open-loop control, (harmonic cancellation technique based on programmed current waveform) closed-loop control including flux and/or torque estimations. The work of Asano, Yoshinari et al. concluded that the vibration of concentrated winding motors tends to be higher than distributed winding motors [37]. Field weakening technique can reduce radial forces in sinusoidally commutated PMBLDC machines [36] but requires higher currents to maintain

the desired torque. Smoothening the drive current to prevent torque ripple can also reduce vibration [37]. Increasing the number of stator phases can also reduce the exciting forces, and hence, the vibration of the machine [35]. Control based methods [17-25], [38, 12, and 15] without influencing the drive hardware can be implemented in a low cost digital signal processor (DSP) and field programmable gate array (FPGA) based motor control hardware; however, the obtained torque is never entirely smooth. Cogging torque is directly related to torque ripple and both of them causes noise and vibration in the machine [17-24]. Radial forces cause significant vibration when they are unbalanced. To improve the performance of a motor, torque pulsations need to be reduced and unbalanced radial forces are to be minimized either by design variation or through control techniques. It is hard to find some designs with low torque ripple and cogging torque as well as with low radial forces. There is always a trade-off among these two phenomena.

3.3 Conclusion

In-spite of the several techniques discussed in this chapter to improve the performance of PMSM, there are still opportunities for further research, especially from a design point of view. The research in this dissertation will show that fairly simple variations in magnet shapes can lead to substantial improvements in torque ripple minimization without sacrificing the average torque significantly. These magnet shape variations can be implemented in a very cost-effective manner. Also, the existing literature showed that magnet skew can reduce cogging torque as well as torque ripple. This research, in particular has shown that this is not always the case and there are ways to utilize appropriate skew techniques. This research will show how the different shapes of magnet for a particular-pole arc can make differences in the peak-to-peak torque ripple in a skewed motor compared to its non-skewed version. It will also show the magnet design cases where torque ripple gets worse even after rotor skewing.

Use of skewed magnets, shifted magnet segments, decentered magnets or selection of magnet width can reduce the cogging torque, and supposedly the torque ripple as well. But, in reality these methods may not necessarily reduce the torque ripple and can even make it worse. It is the dominant order(s) of BEMF harmonics present in those design variations that will determine the reduction or increase of the torque ripple in a skewed motor. Moreover, selection of magnet arc width can eliminate one particular-harmonics of BEMF, but no other BEMF harmonics can be removed. Hence, further research needs to be conducted to see the torque ripple variation (increase or decrease) under magnet skewing for different geometry of PMSM. The determination and elimination of more dominant BEMF harmonics by variation in magnet shapes for one particular slot-pole combination motor with a selected magnet arc width will give a motor design with low torque ripple.

The symmetric arrangement of the magnets by making pole arc equal to pole pitch leads to the maximum value of the fundamental component of the BEMF. However, with this magnet arrangement, the other harmonics of the BEMF are also high to cause a significant torque ripple. In general, a nonsymmetrical distribution of magnets having different pole arc and pole pitch leads to a reduction of the fundamental component of BEMF and also to a variation of the other harmonic components. Therefore, it is possible to find a suitable magnet arrangement leading to a compromise between a high value of the BEMF fundamental component and a low value of all other harmonic components, thus leading to a high-performance motor. Research is thus essential to develop the fundamental understanding of the relationship between magnet shape and BEMF, and then develop the methodology to eliminate certain high order harmonics of BEMF by appropriate shaping of the magnets.

The vibrating tendency of PMSMs doesn't show a direct correlation with the magnitude of the radial stress wave on its stator structure. It also depends on the dominant frequency of the stress wave. Again, it is not only the motor topology (slot/pole combination), but also the winding configuration that determines the lower order frequency of radial stress responsible for vibration. This research is thus motivated to unveil all the above in selecting a PMSM less prone to noise and vibration.

CHAPTER 4

DESIGN METHODOLOGY FOR PMSM

4.1 Introduction

A design methodology for surface mounted PMSM with a given set of design constraints is developed in this chapter. The primary constraints considered are the maximum outer diameter of the stator, the allowable axial length of rotor and stator laminations, the radial depth of the airgap between rotor and stator, the torque and speed requirements and so on. Techniques for reducing cogging torque, torque ripple and radial forces have been incorporated throughout the systematic design approach.

The fundamental steps involved in designing a surface mounted PMSM are described first. The design starts with the specifications that may include the requirements of rated torque T_{rated}, maximum power Pmax or rated speed ω_{mrate}. Supply bus voltage Vbus or dimensions may also be included as constraints. Needless to say that the specifications are application-specific. Aside from the motor design there may exist several other environmental and performance requirements that must be taken into account. The next design steps include the initial selection of the surface mounted PMSM configuration, design parameters and design-ratios (ratios between internal dimensions). Configuration options may include the number of phases, the number of stator and rotor poles, and the number of series or parallel paths in each phase which is also called repetition. Design parameters may include hoop stress Ts, rms current density J_{rms} and rotor torque density $T_{density}$. After selecting the configuration, parameters and design ratios, internal and external motor dimensions such as rotor radius R_g, stack length L_{stk}, stator outer radius Rout etc. are determined through the design equations; an analytical parameter model is then developed to predict the torque ripple and radial forces of the motor. If the output requirements are satisfied, then static and dynamic system level simulations are carried out for verification of overall performance.

4.2 Design Methodology

The electrical machine design is a multi-disciplinary subject. It involves electromagnetic design, engineering materials selection, thermal and mechanical analysis, material and component specifications and production techniques. The magnetic properties of the iron, the numbers of phases and the number of poles-per-phase all have effect on PMSM's performance. These effects along with the sizing of the machine envelope and internal dimensions make the PMSM design an insight intensive effort. In designing PMSM, except for the most basic sizing calculations, the CAD (computer aided design) methods must include system level simulation capability as an integral part of the design

process. Finite element analysis is also needed for the understanding of motor performances at design variations. number of requirements and objectives need to be compromised to achieve an optimal PMSM design for a specific application. Various PMSM design aspects have been studied and reported in the literature [28,29] emphasizing some of the design parameters, the number of phases and repetitions and a few dimensional design ratios. The traditional design process starts with some initial realization derived from experience without going through any optimization routine. One of the main design requirements addressed in this dissertation is torque ripple minimization. This requires the motor to possess a good BEMF waveform (sinusoidal in the case of PMSM) and low cogging torque. Magnet arc length selection and shaping the magnet arc to minimize the BEMF harmonics are necessary to achieve the goals. A further requirement is to maintain lower radial forces to have less radial deflection. This requires correct selection of slot-pole combinations and proper winding arrangements around the stator circumference. A comprehensive design methodology, which sets design guidelines to encompass the effects of machine geometry, configuration and all possible design parameters on the overall performance of the PMSM, will thus, be developed in this research.

Another important part of design is the rotor magnet sizing. The pole arc can be varied with respect to pole pitch and slot pitch or coil pitch to make the flux distribution square wave or sinusoidal as per application requirement (Fig. 4.1).

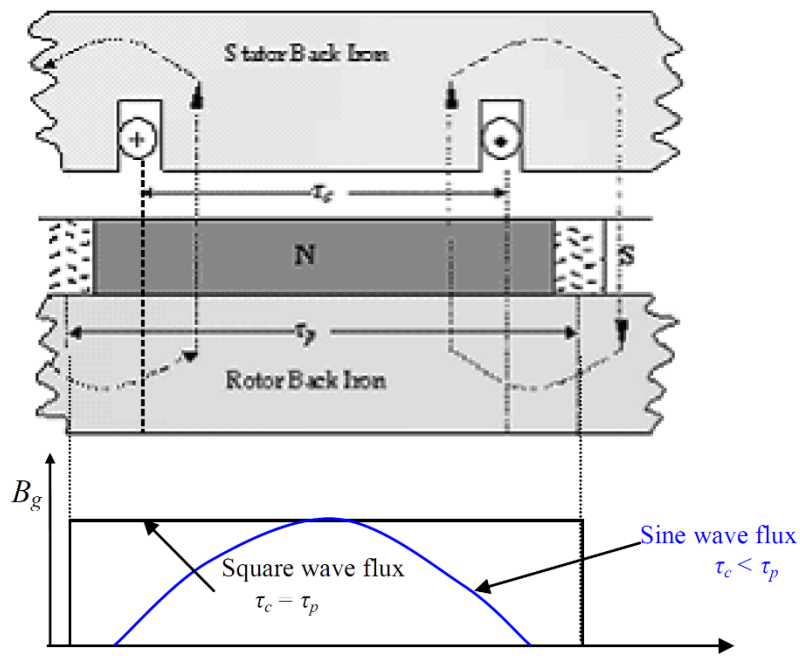

Fig 4.1- Air gap flux distribution pattern for cases when pole pitch and slot pitch are equal and different

A square wave shape of the flux distribution is obtained when $\tau_c = \tau_p$; the flux linked with the winding in this case is

$$\phi_g = B_g . L_{stk} . \tau_p \qquad \text{..... (4.1)}$$

where L_{stk} is the length[32]

Again, the sinusoidal distribution of the flux density is obtained when $\tau_c < \tau_p$; the flux linked with the winding is

$$\phi_g = B_g . L_{stk} . \tau_c = 2 . B_g . L_{stk} . \sin(\theta_{ce} / 2) \qquad \text{..... (4.2)}$$

Here the pitch factor is defined as

$$k_p = \theta_{ce} / \pi = \frac{\tau_c}{\tau_p}. \qquad \text{..... (4.3)}$$

4.3 Design steps

The design steps include the initial selection of the configuration, parameters and dimensional design ratios; evaluation of critical design issues; validation of an “output checklist”; verification of overall performances by system level simulations and finite element analysis (FEA). The design specifications may include all or some of the following parameters depending on the application: rated torque, base speed, maximum rated speed, maximum output power, power factor, supply bus voltage, maximum phase current, torque-ripples, acoustic noise level etc. The number of phases, poles, stator slots as well as winding configuration must be selected based on the application requirements.

The first step is to define the important ratios of the machine dimensions. The design constraints are the iterative process of the design software and simplified output equations are used for the initial sizing and output checklist to simplify the back and forth adjustments of the design variations. The machine configuration, parameters and design ratios are changed within their limits to obtain a satisfactory output checklist for the design. Finally, fine tuning of the design to achieve the accurate static and dynamic performances of the candidate design is carried out through FE analysis of the machine. The design steps are continued in an iterative process until the requirements are met.

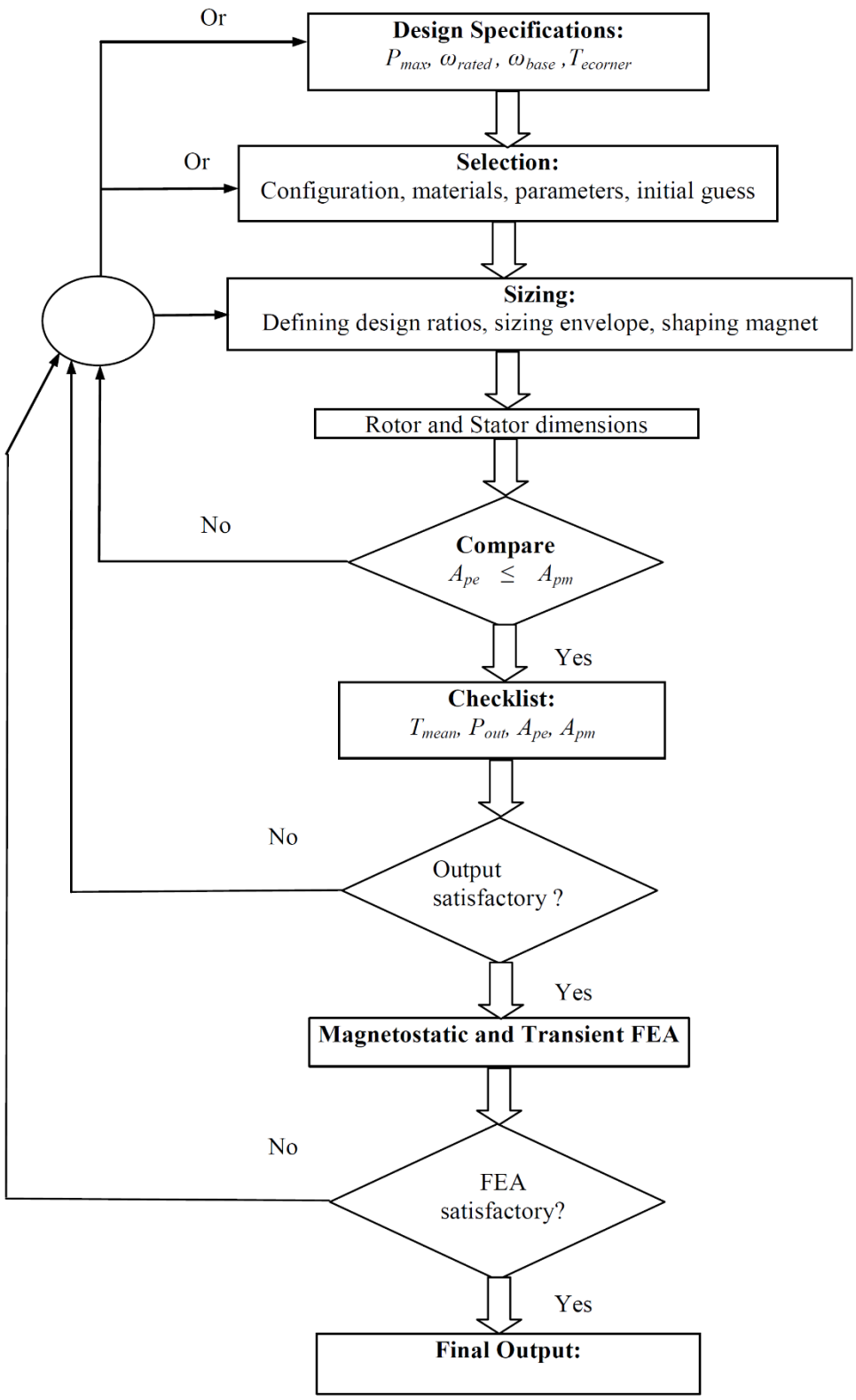

Fig 4.2- Flowchart of the overall design methodology of PMSM.

4.3.1 Design Ratios

The design ratios are defined as the ratios between various internal dimensions of the machine. The objective of defining the design ratios is to maximize the stator mode frequency, to minimize the envelope dimension, and to insure critical speed well above the rated speed of the machine. The ratio between the magnet width, l_m and the slot height, ds (α_{lm}ds) is a comparison between magnetic loading vs. electrical loading, a ratio between magnet size and winding area, and has a significant effect on torque density and mean torque. It indicates a trade off between magnet width and the amount of stator conductors to meet the required torque. The higher the ratio is, the lower is the height of the slot and less would be the number of conductors possible; also, the higher is the thickness of the magnet. The ratio between the outer radius of the stator, Rout and the outer radius of the rotor, R_g (α_{routrg}) is a way of constraining the rotor diameter for a given stator diameter and generally set to 2 as a starting point of design iteration. The objectives for selecting optimal values for α_{lmrg} , α_{routrg} , and α_{lm}ds are to minimize the envelope dimension which is the product of R_{out} and L_{stk}.

4.3.2 Envelope Sizing

Two envelope dimensions of the machine geometry are the air gap radius to the rotor R_g and the axial length of the stack L_{stk}. An initial estimate of air gap radius to the rotor is obtained from the rotor hoop stress and the rated speed of the machine as [42]

$$R_g = \frac{1}{\omega_{rated}} \sqrt{\frac{T_s}{K_h}}, \qquad \text{..... (4.4)}$$

where T_s is the hoop stress and K_h is the hoop stress constant, which is a function of the material property and few design ratios. R_g obtained from this relation gives the maximum allowable dimension for rotor radius to the air gap.

4.3.3 Rotor Torque density

Another important design parameter is the rotor torque density Te_{ρ}, which depends on the saturation flux density (Bsat) of the rotor iron, the type of enclosure, and the cooling process employed in a particular-application. Again it varies inversely with the stack length as

$$L_{stk} = \frac{P_{\max}}{\pi \omega_{corner} R_g^2 T_{e\rho}}. \qquad \text{..... (4.5)}$$

The mean torque density calculated during design iterations is obtained from

$$T_{density} = K_t \frac{J_{rms} A_{wn} B_{sat} STFn_{ser} n_{par}}{R_g} \qquad \text{..... (4.6)}$$

Here, K_t is a constant containing the ratios between the peak and rms values of phase current and torque. J_{rms} is the rms current density that affects a number of design outputs. The mean torque density should be greater than the rotor torque density Te_{ρ}, which should be checked during design iterations. The average torque produced by the machine is proportional to the air gap radius (i.e. rotor radius) squared and to the stack length.

4.3.4 Stator and Rotor Sizing

Once the rotor radius to air gap (R_g) is determined, all other radial dimensions of rotor and stator geometry can be found as a function of R_g and the allowable air gap flux density B_g. The radial depth of stator back iron w_{bi} (also used as y_s), the stator tooth width w_{tb}, and the air gap flux Φ_g is given as

$$w_{bi} = \frac{\phi_g}{2B_{\max} StfL_{stk}}, \qquad w_{tb} = \frac{2}{N_{sp}} w_{bi},$$

$$\phi_g = B_g A_g, \qquad B_g = \frac{B_r}{1 + \mu_r \frac{g_e}{l_m}} \qquad \text{..... (4.7)}$$

The stator radius to yoke R_{ys}, air gap radius of the rotor R_{gs}, and the outer radius of the stator Rout are expressed as a function of the design ratios and rotor dimensions as

$$R_{ys} = R_{out} - w_{bi}, \qquad R_{gs} = R_g + g = R_{ys} - d_s$$

$$R_{out} = \alpha_{routrg} R_g \qquad d_s = d_1 + d_2 + d_3 \qquad \text{.....(4.8)}$$

The selection of the tooth width (w_{tb}) depends on the property of the stator lamination material and the maximum value of the flux density produced in the air gap. The value is chosen such that the tooth doesn't saturate which then can add torque ripple. Another important parameter is the slot opening, w_s. To minimize the value of cogging torque, the slot opening parameter needs to be minimized also. Care should be taken not to make w_s too small, which can lead to slot leakage of the flux and consequently decrease the torque output level. Slot opening is also limited by the winding capability.

4.3.4 Computation of Maximum Number of Turns in the Slot

The rms value of coil current I_{coil} is derived from the expression for maximum Power. Maximum number of turns in the slot ns is then found out as

$$n_s = \frac{A_{slot} . k_{eff} . J_{rms}}{I_{coil}} \quad . \qquad \text{..... (4.9)}$$

The per phase peak current I_{peak} is related to coil rms current as

$$I_{peak} = I_{coil} \times \sqrt{\frac{3}{2}} \qquad \text{..... (4.10)}$$

Maximum allowable slot fill factor based on the winding requirements must be checked prior to determining the number of turns per slot. Therefore, the effective slot area should be used to calculate the number of turns and the maximum amplitude of coil current. Multiplying the slot area by slot fill factor gives the effective area of winding.

$$A_{slot,eff} = A_{slot} . k_{eff} \qquad \text{..... (4.11)}$$

Here, k_{eff} is the slot fill factor expressed as a percentage of the total slot area. This factor depends on the size and shape of the conductor and type of winding mechanism (needle, insert, or segmented winding etc.). A conservative estimate for slot fill factor is between 60% to 70% for needle type of winding with round wire. Care should be taken while maximizing the slot fill either by reducing the wire diameter or by increasing the number of conductors, since both methods will increase the phase resistance.

4.3.5 Number of Phases and Slot/Pole Combinations

The number of phases is mostly application specific. Three phase motors are by far the most common choice for all but the lowest power levels. Common to AC motors, three phase motors have extremely good utilization of copper, iron, magnet, insulating materials and silicon for a given output power. Although the utilization can theoretically be argued to be higher in motors of higher phase numbers, the gains would be offset by the increased number of leads and transistors, which increases cost and may severely compromise reliability.

The maximum number of poles is restricted by the maximum operating speed of the machine to limit the switching losses in the inverter. Again the pole number has to be in pair. The number of slots has to be an integer multiple of number of phases. The selection

of number of stator slots for a given number of poles is crucial to have the minimum effect of cogging torque.
Torque of a brushless PM motor with one slot per pole per phase is approximately given by [28]

$$\tau_{mean} = 2n_s N_m R_g B_g L_{stk} I_{coil} \qquad \text{..... (4.12)}$$

where N_m is the number of magnet poles. This equation suggests that increasing the number of magnet poles increases the torque generated by the motor. A basic rule of thumb is that the number of poles should be inversely proportional to the maximum speed of rotation. The reason, of course, is to limit the commutation frequency to avoid excessive switching losses in the transistors and iron losses in the stator. For very high speeds, two- and four-pole motors are preferred. If smooth torque is required at low speed, such as in a DC torque motor, a larger number of poles should be selected [43]. Yet another consequence of increasing the number of magnet poles is that the required rotor and stator back iron thickness decreases since the amount of flux to be passed by the back iron is reduced. As a result, the overall diameter can be reduced by increasing the number of poles [44]. Another important issue regarding the number of poles has to do with cost. Usually the greater the number of poles, the greater is the cost in magnets and labor for fabrication.

One of the primary constraints on PM stator design is that the total number of stator slots is to be some even integer multiple of the number of phases. There are many combinations of slot- and pole-numbers that can be used effectively [45]. With a large number of slots/pole, the cogging torque is inherently reduced by the fact that the relative permeance variation seen by the magnet is reduced as it successively covers and uncovers the slots one at a time. Also the coil-winding easiness is an important factor for the number of slots or poles. If there is one coil per pole per phase (say, in case of 24 slots and 8 poles), it is then possible to insert all the coils into the stator in one stroke of the machine, which certainly speeds up productions [45]. As suggested in [44], the stator back iron thickness ys is determined by the solution of the magnetic circuit. The flux from each magnet splits equally in both the stator and rotor back irons and is coupled to the adjacent magnets. Thus, the back iron must support one-half of the air gap flux Φ_g, i.e., the back iron flux is $\Phi_s = \Phi_g/2$. If the flux density allowed in the back iron is Bmax, then the back-iron width is

$$y_s = \frac{\Phi_g}{(2B_{\max} L_{stk})Stf} \qquad \text{..... (4.13)}$$

Here Stf is the lamination stacking factor. The typical value between 0.93 to 0.97 is used for Stf .

4.4 Measurement for Torque pulsations

The most effective technique to minimize the torque ripple is through the motor design. Skewing is one of the good option to minimize the torque ripple with the trade-off of the high motor construction cost. But instead of skewing we do have so many other techniques such as current harmonic injection method and hybrid magnets method etc. Torque ripple is hard to measure or estimate, usually pulsations can be estimated by three techniques: electrical measurements, the machine design parameters and simulations, or mechanical measurements.

4.4.1 Electrical measurements

At the shaft ,Torque pulsations cannot be exactly measured ,there are other methods exist to quantify them. Because of space harmonics created by the machine geometry we have torque pulsations. As a reflection of these space harmonics we have harmonics in the back emf, this allows the use of this measurement to estimate the current harmonics needed to cancel pulsating torques. One of the most popular techniques is to estimate the electrical torque from the voltages and currents measured at the terminals. These methods needs measurement and storage of back emfs ea,eb,ec, at various speeds. An estimate of the electrical torque equation can then be calculated or figured in real time from the on-line currents (ia,ib,ic) and shaft speed ωm

$$T_{em}(t) = \frac{1}{\omega_m}[e_a(t)i_a(t) + e_b(t)i_b(t) + e_c(t)i_c(t)] \qquad \text{..... (4.14)}$$

Transforming the back-EMF and current information to the d-q reference frame to assess electrical torque equation 4.15 , offers advantages particularly when making assumptions to generate current references.

$$T_{em} = \frac{1}{\omega_m}\frac{3}{2}[e_d i_d + e_q i_q + e_o i_o] \qquad \text{..... (4.15)}$$

In a combined off-line measurement of back-EMF and advance knowledge of saliency properties of IPM machine are utilized to compute torque using equation 4.16, for a Pn pole machine. This methods reports for the harmonic content due to
the embedded magnets and presumes static values of the Ld and Lqinductances

$$T_{em} = e_q i_q + P_n(L_d - L_q)i_d i_q \qquad \text{..... (4.16)}$$

The back emf in the rotor frame is given by

$$e_d = \omega_r[A_1 \cos(-\varphi_1) + A_5 \cos(6\omega t - \varphi_5) + A_7 \cos(7\omega t - \varphi_7)] \quad \text{..... (4.17)}$$
$$e_q = \omega_r[A_1 sin(\varphi_1) + A_5 \sin(6\omega t - \varphi_5) - A_7 sin(7\omega t - \varphi_7)]$$

Torque ripple information could be obtained from the terminal quantities but the obtained information can be limited based on machine assumptions. The back-EMF provide a first order model of the space harmonics in the air-gap, but the terminal voltages may not exhibit an exact relative connection due to the interaction of current and rotor MMF. It is hard to choose position dependent inductance information from the terminals, making reluctance torque ripple not that easy to treat. The actual EMFs seen under loaded conditions may not match the back-EMF measurements made off-line.

4.4.2 Mechanical Measurements

Usage of strain gauges based on Hooke's law are the most usual methods to measure the mechanical torque at the shaft. Latest hard-wired rotating measurement methods, include using slip rings based on the same principal as SG. based on the same SG principle a rotary transformer torque cell is too used where the secondary of the transformer keeps rotating. Load cells would be used to evaluate the torque by measuring the changes in a moment arm positioned outside the motor casing. Other non-contact strategies include twin beam torque cell or clamp-on torque cell which works on the wireless measurement principle. The clamp-on torque cell may be pre-calibrated bending beam mounted between two collars that clamp on the shaft. Wireless torque cells that contains of a rotary torque transformer connected in-line with typical industry flanges also being used. Most of these ways suffer from noise interference and vibrations within the measuring that makes them unreliable. Another disadvantage of utilizing these methods is that the torque pulsations would be suppressed in the measurements by machines with high inertia. Future measurement strategies could embrace the utilization of smart sensors and other alternative new technologies

4.4.3 Simulation and analysis

Exact estimates of the torque pulsations will be acquired using details of the precise machine geometry or electrical parameters. Quantities like the stator MMF, rotor MMF, inductance, and linear current density has spatial variations that rely on the rotor position. The geometry provides sufficient information to from a Fourier series illustration of the air gap flux density and linear current density. High frequency components in these quantities lead to torque pulsations. Information of however the inductance varies with rotor position and current magnitude may also be utilized to estimate torque pulsations.

Upon breaking down every flux linkage component, in the equation(4.18), the flux is relies on the inductance. With constant d and q axis current commands, the ensuing torque contains pulsations because of non-constant inductances.

$$\lambda_q = L_q i_q$$
$$\lambda_d = L_d i_d + \lambda_{pm} \qquad \text{..... (4.18)}$$

Finite Element will give more accuracy in the machine model as a result of it includes iron saturation and leakage flux effects. Mechanical parameters may also be used to calculate torque pulsations. Under these presumption that the inertia (J), friction (B) and load torque (T_L) are acknowledged parameters and speed feedback (ω) is provided, the exact torque waveform can be measured using (4.19). These parameters are not computed from the machine design, but if they were exactly known then an accurate torque measurement is possible.

$$T = J\frac{d\omega}{dt} + B\omega + T_L \qquad \text{..... (4.19)}$$

4.5 Motor design

According to the motor design point of view skewing the stator lamination stacks or rotor magnets, organizing proper winding distribution reduces cogging torque to a significant limit but do not completely abolished. Further, prominent machine design processes additionally increase the complexity in the process of production and also increase the cost of the machine. Recursive least square (RLS) estimation algorithm is used to compute parameters of inductances for Interior Permanent Magnet Synchronous Motor (IPMSM). This control method can lessen torque ripple of IPMSM due to keeping linearity of inverter output[72].

A technique called flux estimation is used to approximate the rotor position of the slot less PMSM that takes benefit of the slot less machine's characteristically low inductance to limit the flux estimation error. The rotor position is approximated taking a reference model and the measured phase currents and voltages. The suggested sinusoidal control method reduces the torque pulsations existing when Hall sensor position feedback alone is used and abolishes the need for high-resolution rotor angle sensors. The benefit of this method is that it doesn't need to know the structure specifications, the torque internal motor mechanical ripples are reduced by 91 percent. So the designers have the capability to utilize motor with high torque to volume ratio and low-cost motor without taking considering the cogging problem. Permanent magnet torque ripple rely on the selection of the permanent magnet width and the slot opening width. The torque ripple tends to

possess a minimum for one or two completely different permanent magnet width, relying on the number of slots per pole per phase. This method reduces or lessens the third harmonics of air gap flux density. [72]

4.6 Design of controller

Many controllers had been utilized to minimize the ripples. Sliding-mode control is one of the controllers of them is sliding mode control which depends on a generic mathematical model of the motor. The approximation is relied on the differentiation of measured signals basing the schemes of robust exact differentiator (RED). This is executed on an industrial servo drive. This planned technique with two PI controllers to suppress the harmonics, torque ripples, noise and electromagnetic interference. Invert switching frequency is affected by PI controllers which also reduces the cogging torque. Permanent magnet synchronous motors offers a smooth operation for giving a smooth waveform of current and torque.

Many [73] of the researches has the source of the energy as electrical energy. However this method makes use of fuel cells as a source of energy. A fuel cell supplying a boost converter which moreover supplies a three phase tri-state CSI which gives rise to minimized torque ripple, which has been proved in Hybrid Electric Vehicle.[72] To minimize the torque ripple we had another algorithm we use that is Direct torque control. The electromagnetic torque in a Permanent magnet synchronous motors is proportionate to the angle in between the stator and rotor flux linkages. Direct Torque Control(DTC) issues a good dynamic response and its main benefit of Direct Torque Control is its structure which is simple. An improved Permanent magnet synchronous motors Direct Torque Control strategy by utilizing an active null vector modulation strategy based on an rms torque-ripple equation minimization. The suggested scheme improves the performances of Direct torque control by mixing low torque ripple characteristics in steady state with the faster torque dynamics. The application of tooth shape optimization process for cogging torque can be reduced in permanent magnet motors. An optimum tooth shape has been obtained by the illustrated algorithms[74].

The suggested method effectively reduces the torque ripple caused by the magnetic saturation at the rated torque. In this process an effective real time inductance measurement procedure makes use of the DFT was tendered to acquire the inductance distribution in accordance with rotor position. The magnetic saturation of the Permanent magnet synchronous motor was validated by this measurement procedure. Further, the saturation effect was reviewed by a nonlinear analysis, and a simple active cancellation strategy to reduce the torque ripple at every electric angle was proposed.

The sensor less control of the interior-magnet motor is relied on a speed-adaptive observer increased with a pulsating high-frequency signal injection procedure at very low speeds. The suggested method for torque ripple reduction is appropriate for sensor less Permanent magnet synchronous motor drives. Taking both flux harmonics and inductance harmonics into account, and a harmonic in the torque calculation is suppressed using a torque ripple compensator depending on three additional motor parameters[74].

Torque ripples are also caused by offset error and scaling error. These ripples degrades speed control performance. A compensation technique is made use to acquire precise torque control and remove ripples in speed. Basic analysis has shown that the both offset current and scaling error causes the torque error oscillating at the frequency .By this method ripples are reducedto some wanted extent.

An reduction of torque ripples of an interior permanent magnet motor drive with adaptive-filter-based torque-ripple minimization of a fuzzy-logic controller for speed control. Based on the magnitude of the torque ripple we adapt the gain of the filter. The optimal position of the filter in the complete drive is also governed for effective Torque ripple minimization.

A DTFC space vector based on PWM technique is suggested to minimize the ripple in torque, flux and current in the steady state. A new approximation for speed control of PMSM servo system based on fuzzy logic technique. Without modifying the motor parameters and load a fuzzy logic-based DTC methodology is utilized for an efficient control of the torque and flux.
In torque ripples reduction we had a great reduction through adaptive controller when compared with other controllers by enabling speed tracking while minimization of the torque ripple.
A hybrid filter topology is suggested to reduce torque pulsation by using direct torque hysteresis controllers of switching voltage harmonics and EMI noises in permanent magnet synchronous motors. The AF is characterized by detecting the harmonics in the motor phase voltages and uses hysteresis voltage control method to give almost sinusoidal voltage to the motor windings. The simulation results of this combined control structure depicts considerable torque ripple or pulsation reduction in steady state range and adequate dynamic torque performance as well as harmonics which can be considered and EMI noise reduction.[74]
In time domain to reduce periodic torque pulsations an iterative learning control scheme is implemented. But this limited the extent to which torque pulsations can be suppressed. In-order to remove this limitation, an altered ILC (Iterative Learning control) procedure was implemented.

4.6 Soft computing design

Soft computing techniques were used to reduce the torque ripples in Permanent magnet synchronous motors. For this type of motors, Neural controller is utilized for torque ripple minimization. We used two methods of neural controller design. The first method is based on current controller and speed controller. The second method is based on estimation of torque constant and stator resistance in Permanent magnet synchronous motor. The q-axis inductance is modelled off-line according to q-axis stator current. Weights are initially taken as small arbitrary value and those weights are modified according to the model reference control algorithm.[72]

A novel compensation method for permanent magnet synchronous motor direct torque controlled (DTC) drive based on neuro-fuzzy observer is suggested. Instead of conventional hysteresis controller two Fuzzy logic controllers are used. This method presents the implementation of a voltage distortion observer based on the artificial neural network (ANN) and produce a torque without ripple. [72] In latest period, to minimize the torque ripples we made use of direct torque control along with soft computing techniques. The application of vector control and direct torque control (DTC) with neural network to reduce the ripples.

A DTFC space vector based on PWM technique is suggested to minimize the ripple in torque, flux and current in the steady state. A new approximation for speed control of PMSM servo system based on fuzzy logic technique. Without modifying the motor parameters and load a fuzzy logic-based DTC methodology is utilized for an efficient control of the torque and flux.

Non-dominated Sorting Genetic Algorithm is used to reduce cogging torque in PMSM. NSGA is a Multiple Objective Optimization algorithm. The goal of algorithm is to reduce the peak value of cogging torque while the average air gap flux density remains unaltered. Also, the algorithm tries to lessen the area of the magnets. In each iteration of GA, Finite Element Method (FEM) is used to estimate the cogging torque and to acquire the air gap flux density in this study. The results have shown that the cogging torque is reduced by more than 10 times using suggested method.[72]

4.7 Conclusion

Use of skewed magnets, shifted magnet segments, decentered magnets or selection of magnet width can reduce the cogging torque, and supposedly the torque ripple as well. But, in-reality, these methods may not necessarily reduce the torque ripple and can even make it worse. It is the dominant order(s) of BEMF harmonics present in those design variations that will determine the reduction or increase of the torque ripple in a skewed motor. Moreover, selection of magnet arc width can eliminate one particular harmonics of BEMF, but no other BEMF harmonics can be removed. Hence, further research needs to be conducted to see the torque ripple variation (increase or decrease) under magnet skewing for different geometry of PMSM. The determination and elimination of more dominant BEMF harmonics by variation in magnet shapes for a particular slot-pole combination motor with a selected magnet arc width will give a motor design with low torque ripple. The symmetric arrangement of the magnets by making pole arc equal to pole pitch leads to the maximum value of the fundamental component of the BEMF. However, with this magnet arrangement, the other harmonics of the BEMF are also high to cause a significant torque ripple. In general, a nonsymmetrical distribution of magnets having different pole arc and pole pitch leads to a reduction of the fundamental component of BEMF and also to a variation of the other harmonic components. Therefore, it is possible to find a suitable magnet arrangement leading to a compromise between a high value of the BEMF fundamental component and a low value of all other harmonic components, thus leading to a high-performance motor. Research is thus essential to develop the fundamental understanding of the relationship between magnet shape and BEMF, and then develop the methodology to eliminate certain high order harmonics of BEMF by appropriate shaping of the magnets.

The vibrating tendency of PMSMs doesn't show a direct correlation with the magnitude of the radial stress wave on its stator structure. It also depends on the dominant frequency of the stress wave. Again, it is not only the motor topology (slot/pole combination), but also the winding configuration that determines the lower order frequency of radial stress responsible for vibration. This research is thus motivated to unveil all the above in selecting a PMSM less prone to noise and vibration.

A comprehensive design methodology for PM machine has been presented in this chapter. The critical factors of torque ripple and cogging torque have been discussed. The next chapter will present novel PMSM design techniques to minimize torque ripple. One of the contributions of this research is the pole shaping and rotor skewing techniques to reduce cogging torque and hence torque ripple. Several design techniques will be applied to manage the torque ripple issues; both test and simulation results for some of these designs are documented in the next chapter.

CHAPTER 5

REDUCTION TECHNIQUES

5.1 Introduction

Permanent magnet synchronous machines are vulnerable to significant amounts of torque ripple if they are not carefully designed. Even though minimizing cogging torque can help reduce the torque ripple but cannot definitely give rise to a low-level torque ripple. This chapter presents some solutions for minimizing the cogging torque and suppressing operation torque ripple simultaneously. This may be reduced, where a magnet with different width is used so that the flux density distribution in the machine is substantially changed. The magnet widths for minimizing cogging torque can be obtained by using an analytical model. The influence of magnet widths on operation torque ripple and average operation torque is examined by using Finite Element Analysis (FEA) which gives more preciseness to calculations. It is found that the cogging torque and operation torque ripple can be greatly reduced, but with slight average output torque reduction. At last, the Unbalance Magnetic Pull (UMP) is examined, indicating that the presented method can substantially increase the UMP due to the asymmetric distribution of magnets.

Interior permanent magnet synchronous machine (IPMSM) has been widely used in industrial applications in recent years for high power density, high efficiency and high, power factor. However, some drawbacks such as large cogging torque and large torque ripple during operation affect system performance and limit the applications of IPMSM. Skewing is the most common and effective method to reduce the cogging torque, but it increases manufacturing cost. [46] The cogging torque is the consequence of the interaction between of the permanent magnets field and the stator slots, which produces reluctance variations with the rotor position, and it is independent of stator current. The PM torque ripple is the result of interaction of air-gap flux density high harmonics generated from the rotor magnets and stator winding.

One of the main requirements during a new motor design for industry application is the low torque ripples and low cogging torque. For automobile application the torque ripple and cogging torque should be lower than 5% and 0.5% of the nominal torque, respectively. In several papers, numerous methods for reducing torque pulsations components, such as the magnet pole arc design, skewing of rotor magnets or stator slots, dummy slots, PM shifting, different slot width pairing etc., have been proposed and investigated in this chapter. [47]

5.2 Cogging Torque and Torque Ripple Reduction of IPSM Using Asymmetric Flux Barriers

In order to reduce the torque ripple, three configurations of flux-barriers are presented. Fig 5.1 shows the geometric parameters of the flux-barriers parameters under one pole pair which need to be optimized. The torque ripple varies with the distances from the tips of flux-barriers to the axis. This is because the magnetic saturation can be changed by the flux-barriers. In general, the flux-barriers of rotor are symmetric, i.e., $d_1 = d_2 = d_3 = d_4$. But the proposed three asymmetric flux-barrier configurations can have different values of d_1, d_2, d_3 and d_4. This means that there are more degrees of freedom when optimizations are carried out so that the torque ripple can be better reduced. Three prototype IPMSMs are designed, according to the follower flux-barrier configurations: Motor I - $(d_1 = d_3) \neq (d_2 = d_4)$, Motor II – $d_1 \neq d_2 \neq (d_3 = d_4)$ and Motor III - $(d_1 = d_4) \neq (d_2 = d_3)$. All these models are analyzed and optimized with FEM. The optimal values of d_1, d_2, d_3 and d_4 which can minimize the torque ripple at full load are listed in Table 5.1

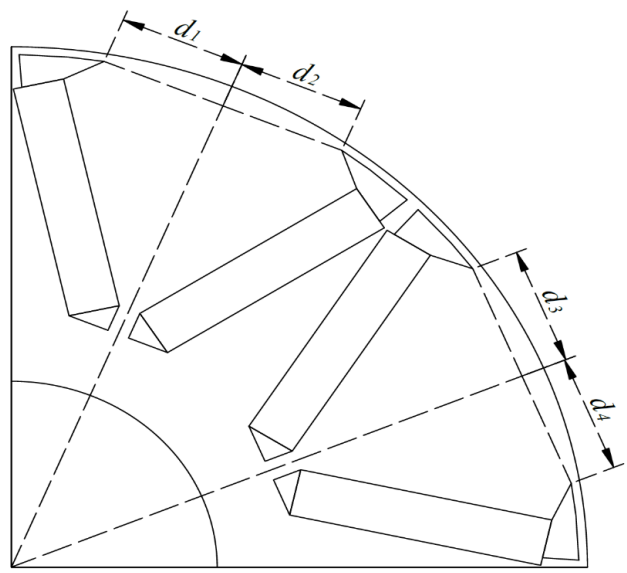

Fig 5.1 Parameters of flux-barriers to be optimized.

5.2.1 Analysis of Torque Performance

The torque performance of the initial motor and the Motors I, II and III is analyzed and compared. The electromagnetic torque under rated load and the cogging torque are showed in Fig. 5.2 a&b, respectively. And Table 5.2 reports the comparison of the average torque, the operation torque ripple and the cogging torque, where T_{avg} means the average torque under full-load condition, T_{ripple} is the peak-to-peak value of the operation

torque ripple under full-load condition and T_{cogging} means the peak-to peak value of the cogging torque under no-load condition. Clearly, the initial motor should have the same torque performance in the CCW and CW rotating directions. Therefore, the small difference of its torques in Table 5.2 is caused by the FEM calculation error, which is negligible. Such error exists in the calculation for the other three motors.

	d_1	d_3	d_3	d_4
Initial motor	15.3mm	15.3mm	15.3mm	15.3mm
Motor I	14.6mm	15.3mm	14.6mm	15.3mm
Motor II	14mm	15.9mm	15mm	15mm
Motor III	13.5mm	15.9mm	15.9mm	13.5mm

Table 5.1 Optimal values of flux-barrier parameters

Rotation direction	Parameter	Initial motor	Motor I	Motor II	Motor III
CCW direction	T_{avg} /Nm	77.56 =	77.33	77.32	77.34
	T_{ripple}/Nm	9.66 =	4.41	3.24	5.71
	$T_{cogging}$ /Nm	6.34 =	4.26 =	5.84 =	4.02 =
CW direction	T_{avg} /Nm	77.71	77.68	77.52	77.49
	T_{ripple}/Nm	9.44	11.67	12.43	5.94
	$T_{cogging}$ /Nm	6.34	4.24	5.73	3.86

Table 5.2 Comparison of average torque and torque ripple under different conditions

In Table 5.2, the sign "=" shown in the CCW direction means that the torque performance should be the same as in the CW direction if the FEM calculation error is discarded. As we can see, the torque ripple is significantly reduced by the proposed configurations of flux-barriers, and the cogging torque is reduced, too. Moreover, the average torque only decreases by ~0.2Nm, which can be ignored. Among these proposed motors, Motor I and Motor II show excellent on-load torque performance in the CCW direction, although their cogging torque does not decrease significantly. It should be pointed out that it is the operation torque ripple but not the cogging torque that affect the motor actual operation.

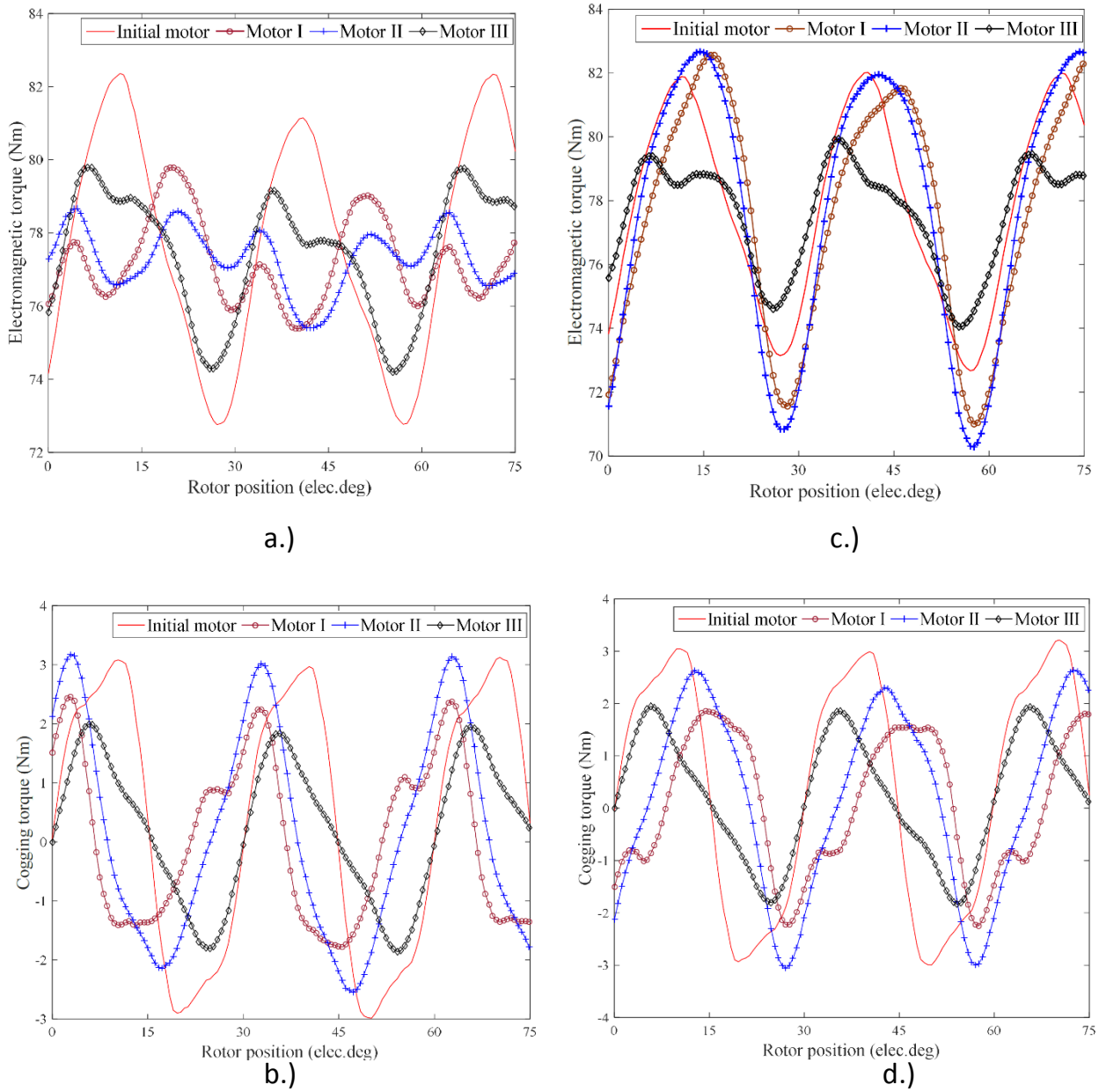

Fig 5.2 a.) Electromagnetic torque under full-load condition in CCW direction. b.) Electromagnetic torque under full-load condition in CW direction. C.) Cogging torque under no-load condition in CCW direction. d.) Cogging torque under no-load condition in CW direction.

What's more, due to the asymmetric structure of each pole pair, the on-load torque performances of Motor I and Motor II are different in the other rotation direction (the CW direction), while the cogging torque are not affected, as Fig. 5.2 c & d show.

When the machines rotate in the CW direction, their electromagnetic torque performance becomes worse than that of the initial one. So they are just suitable for

applications where the machines rotate in a direction. However, most industrial applications require smooth output torque in both rotation directions, calling for a relatively symmetric rotor, thus Motor III is proposed. When considering the operation torque ripple, Motor III performs slightly worse than Motor I and Motor II, however, its torque ripple still decreases by 41% and its cogging torque decreases by 36.6% when compared with the initial motor. Moreover, its torque performance is not affected by the rotation direction, as can be seen from Table 5.2. This is because, in Motor III, the flux-barriers of any pole are symmetric to the flux-barriers of the neighboring pole against the q-axis between these two poles, although the flux-barriers inside each pole are asymmetric to each other against the d-axis of that pole. Clearly, the situation of Motor I and Motor II is different, hence, Motor I and II perform differently into the two rotating directions. In sum, all the three configurations of flux-barriers can reduce torque ripple and cogging torque effectively. But Motor I and Motor II are just suitable for a single fixed rotation direction, while Motor III is suitable for both directions. [48 & 49]

5.2.2 ANALYSIS OF RELUCTANCE TORQUE RIPPLE

In order to investigate the influence of the proposed method in depth, FPM is used to analyze and compare the performance of the reluctance torque between the initial motor and the three proposed motors. The results are given in Fig. 5.3. As we can see, the reluctance torque ripples of Motor I and II are almost unchanged compared with the initial one, decreases by ~0.46Nm and ~0.22Nm, respectively. However, the influence on Motor III is relatively larger, as the reluctance torque ripple decreases by ~1.58Nm, say, 28.6% of the initial reluctance torque ripple [50 & 51].

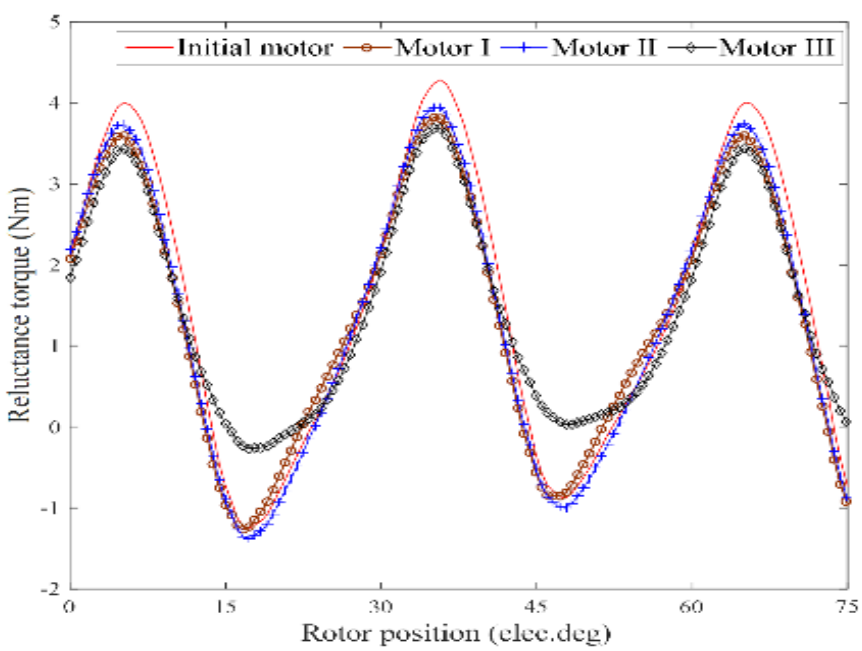

Fig 5.3 Reluctance torque under full-load condition in CCW direction

However, compared with the total reduction of electromagnetic torque ripple, the reduction of reluctance torque ripple of Motor III occupies a relatively small ration, about 40% of the total decrease of operation torque ripple, but the reduction of the former two motors are even small, by only 8.8% and 3.4%, respectively. This means that the method of employing asymmetric flux-barriers is not suitable for machines of which torque ripple is mainly composed of the reluctance torque ripple, such as the PM assisted synchronous reluctance machines (SynRMs). On the other hand, these asymmetric flux-barrier configurations are quite suitable for those machines which mainly suffer from the PM torque ripple and the cogging torque.

5.3 Unequal Teeth Widths for Torque Ripple Reduction in Permanent Magnet Synchronous Machines with Fractional-Slot Non-Overlapping Windings

Usually, the stator in a PMSM is made of laminated steel with high-magnetic permeability. However, this material has non-linear B–H curve, which represents the permeability reduction at higher flux density values in the steel. The synchronous inductance variation in TCW PMSMs causes torque ripple, and that its harmonic order determines the harmonic order of the torque ripple. From this information, it can be concluded that it is preferable to keep the synchronous inductance constant, or to eliminate low-order harmonics of the synchronous inductance variation, because high-order harmonics of the torque ripple are less harmful compared with the low-order harmonics [52, 53].

PMSMs with rotor surface permanent magnets, the flux density peaks in the adjacent stator teeth can have different values, which leads to different teeth permeability and, as a consequence, to the synchronous inductance variation. This phenomenon can cause torque ripple in the PMSMs.[54] The saturation effect in the stator side can indeed have a significant impact on the total torque ripple. However, other high-order harmonics remained approximately at the same level and were not affected by different steel properties (except slightly different cogging torque). Therefore, mainly the 6th-torque ripple harmonic is affected, because the oversaturation in the phase occurs two times per electrical period. The machine has three phases, which means that the affected torque ripple harmonic is $2 \times 3 = 6$. It should be noted that no changes were made to tune the air-gap flux density by permanent magnets, during the optimization process, but only the stator geometry adjustment is considered. This means that if the 6th-torque ripple should be eliminated, the torque ripple by saturation effect can be adjusted to compensate the torque ripple by the non-ideal sinusoidal waveform of the back EMF. f the widths of the adjacent stator teeth are redesigned in a way that they have approximately the same peak flux density, it is possible to reduce or even fully eliminate some harmful harmonics of the torque ripple. Three different TCW PMSMs were analyzed using FEM—12-slots 10-poles PMSM with outer rotor and surface permanent magnets

[54], 144-slots 120-poles PMSM with inner rotor and rotor surface permanent magnets, and 18-slots 16-poles with inner rotor and rotor embedded permanent magnets [55, 56]. The outer rotor 12-slot 10-pole PMSM was originally designed for a blower application. This type of an application requires silent work, which together with tuning of the radial force (reduction of the radial force strength and elimination of its low-order harmonic components) also demands a low-torque ripple.

The widths of the stator teeth were changed that at the nominal load they have approximately the same flux density peaks, as shown in Fig 5.4. It should be noted that the width of one stator tooth was increased to the same extent as the width of the second tooth was decreased, or in other words the slot width (area) remained unchanged. In addition, skewing is implemented in the same way, as shown in Fig 5.4, which in theory should eliminate or reduce the 6th, 12th, and 24th harmonic components in the cogging torque and torque ripple.

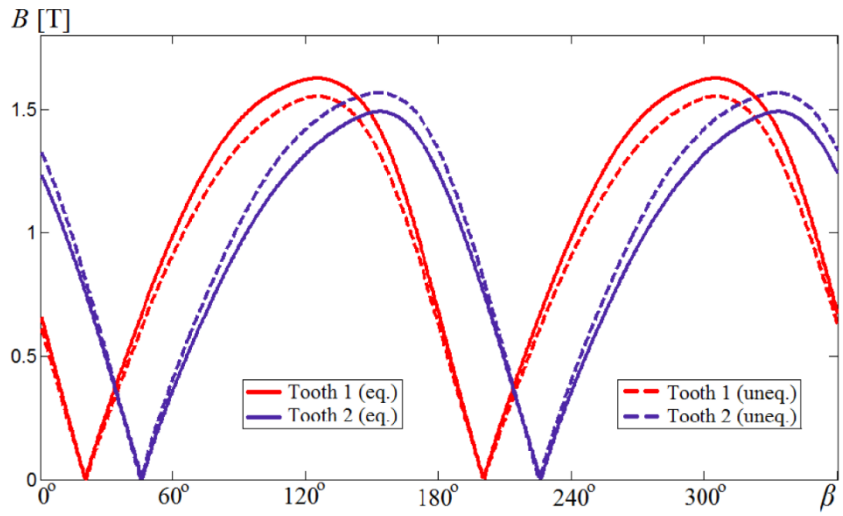

Fig 5.4 Flux densities in the stator teeth of the original 12-slot 10-pole PMSM (with equal teeth widths) and of the redesigned PMSM (with unequal teeth widths) at the nominal load.

The torque curves at the nominal load of the original motor and of the redesigned motor with and without skewing are shown in Fig 5.5 with the spectrum analysis. For simplification purposes each design solution is marked as (γ = skewing angle, Uneq. Or Eq., number of pcs), where γ shows the skewing angle (if skewing is assumed continuous), Unequal. Or Equal. determines if the stator teeth have unequal or equal widths, and number of pcs shows how many divisions the permanent magnets have along the axial direction.

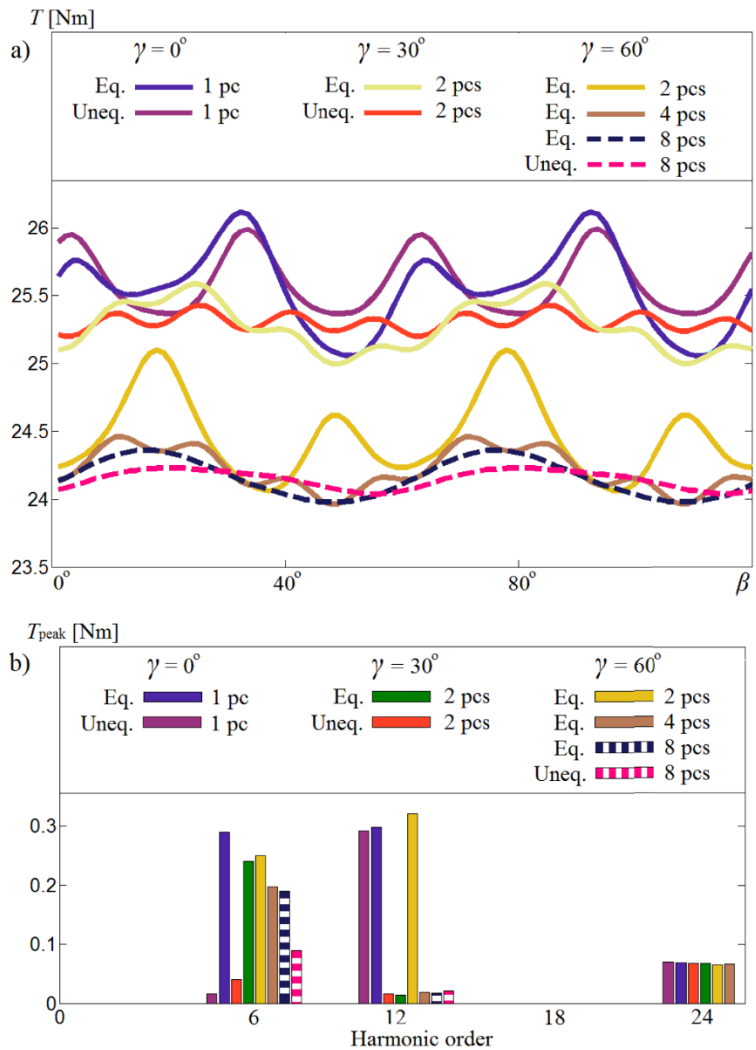

Fig 5.5 a) Torque curves of the skewed and non-skewed original 12-slot 10-pole PMSM (with equal teeth widths) and of the redesigned PMSM (with unequal teeth widths) at the nominal load. (b) Spectrum analysis of the torque curves.

In Fig 5.5, it can be seen that implementation of only unequal teeth widths can eliminate the 6th-torque ripple harmonic at the nominal load (γ = 0°) compared with the original design (γ = 0°). In addition, it is possible to eliminate 12th and 24th-torque ripple harmonics using skewing (γ = 30°, Eq., 2 pcs), (γ = 30°), (γ = 60°), (γ = 60°), (γ = 60°), and (γ = 60°). However, as observed in Fig 5.5, the skewing does not eliminate the 6th-torque ripple harmonic. The situation was similar to the one described in [57]. It is possible to achieve a reduction of the 6th-torque ripple harmonic, if the permanent magnets are divided into more than two parts during the skewing (γ = 60°), (γ = 60°),

and (γ = 60°),but the total elimination of this harmonic is not possible if only skewing is implemented. The reason of this is the fact that skewing divides the machine in axial direction on several parts, where each part has different interaction of the armature flux with permanent magnet flux, due to different phase shifts of the fluxes created by the armature current linkage and permanent magnets along the axial direction. As it is shown previously, this is the main reason of the unequal maximum saturation levels in the stator teeth (1) and (2). In other words, there is different saturation level in the stator teeth in the axial direction, if the skewing is implemented. Therefore, it is suggested that if the 6th-torque ripple harmonic should be eliminated or significantly reduced, the technique with unequal teeth widths described in this paper should be implemented without skewing (γ = 0°). However, in this case other torque ripple harmonics retain their presence.

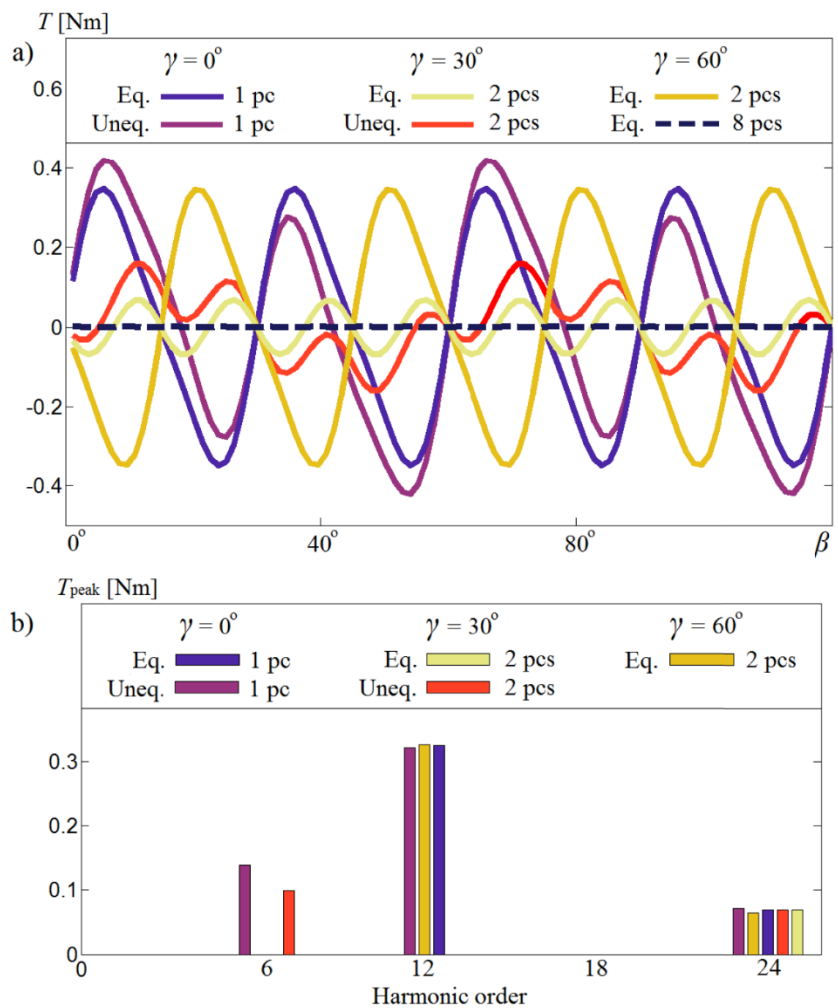

Fig 5.6 a) Cogging torque curves of the skewed and non-skewed original 12-slot 10-pole PMSM (with equal teeth widths) and of the redesigned PMSM (with unequal teeth widths) at no-load. (b) Spectrum analysis of the torque curves

The no-load cogging torque curves for different PMSM design solutions are shown in Fig 5.6. The cogging torque can be eliminated using skewing technique, without any additional approaches, due to the fact that there is no armature reaction at no-load [57]. In Fig 5.6 and Table 5.1, it can be seen that a particular cogging torque harmonic is eliminated, if the angle (in electrical degrees), which takes half of the period of this harmonic is divided by angle (α) between two adjusted permanent magnets of the skewing gives integer value. For example, if the 12th cogging torque harmonic is needed to be eliminated, the permanent magnets should be divided in the axial direction, so that the angle between two adjacent permanent magnets is 15 electrical degrees.[57] Some torque waveforms for different PMSM geometry solutions are not shown in Fig 5.6, because they are near to fully coincide with other (shown) torque waveforms. For example, (γ = 30°) at no-load has the same cogging torque behavior as (γ = 60°), and (γ = 60°) does not have any practical cogging torque as well as (γ = 60°). However, all the simulated torque harmonic components for different design solutions can be found in Table 5.1. It should be noted that the described 12-slot 10-pole PMSM was analyzed with current supply. Therefore, the purely sinusoidal current was conducting in the stator windings. In this case, the local saturations, which causes synchronous inductance variation, should influence the voltage waveform of the current supply. However, the saturation in the stator teeth varies at different teeth widths, which leads to the synchronous inductance variation and consequently to the load angle change for the same working point. For example, to keep the same torque as of the original PMSM, the load angle δ of the redesigned wind generator was reduced from 52 to 50 electrical degrees. It means that the generator with unequal stator teeth has ~3% higher overload capability than the original design.

The limitation of using the unequal teeth widths approach comes from the fact that, if the teeth widths are optimized, to have approximately equal flux density peaks in the stator teeth at one working point, they are not the same at other loads, because in this case the armature reaction (flux created by the armature current linkage) is different. It means that the 6th-harmonic order of the torque ripple is not completely eliminated at other working points. Therefore, the stator teeth widths optimization should be implemented with the knowledge of the prevailing loads. It is also shown that with negative torque (when Iq is negative) the torque ripple increases to the same extent as with positive torque in case of equal teeth widths, but with higher extent with the unequal stator teeth widths, due to the same reason (different armature reactions). It was found that in TCW PMSMs, the 6th-torque ripple harmonic is partially produced by non-symmetrical peak flux density distributions in the stator teeth, due to interaction of the permanent magnet flux with armature flux. The 6th harmonic can be eliminated by teeth widths adjustment, whereas conventional skewing technique is not appropriate for the reduction of this

harmonic. However, skewing is still favorable for the elimination of cogging torque in TCW PMSMs.[58] The main disadvantage of the method with unequal stator teeth is that it gives the desirable results for only one working point, whereas for other loads the 6th-torque ripple harmonic increases. The described methods can be used by designers, which should be aware of these local saturations in TCW PMSMs, especially when low-torque ripple is one of the design targets.

5.4 Cogging Torque Minimization and Torque Ripple Suppression in Surface-Mounted Permanent Magnet Synchronous Machines Using Different Magnet Widths

In Surface-mounted PMSM, all the magnets normally have the same dimensions and the interval spaces between two adjacent magnets are also the same, as Fig 5.7(a) shows.

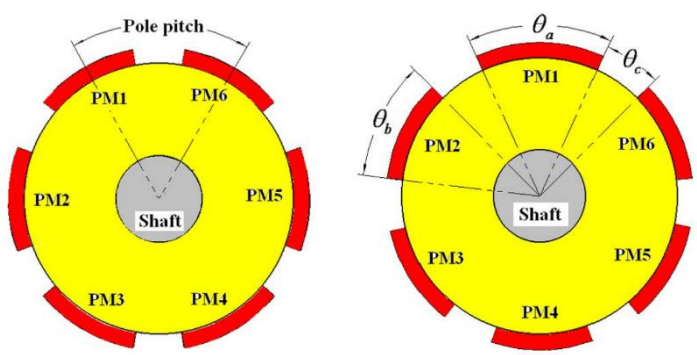

a.) b.)

Fig 5.7 Cross section of rotor of surface mounted PMSM. (a) Uniform magnet rotor. (b) Different magnet widths method.

The method of different magnet widths presented in this chapter is shown in Fig 5.7(b). The width of one magnet is θ_a whereas that of other 2p-1 magnets is θ_b, p is the number of pole pairs. The interval space between two magnets is θ_c. For convenient illusration, we defined α_p as the pole arc to pole pitch ratio before using the method, k_t is defined as the widths ratio, $k_t = \theta_b / \theta_a$. If α_p is given, θ_a and θ_b can be obtained according to k_t. When k_t=1, all the magnets are of the same width, thus have a uniform rotor. Note that there are two salient points for this presented method:

1) The total magnet material mass consumed is not changed before and after using the method, this is important for inspecting the cost of the machine.
2) The method can be applied to a machine in case that the pole arc to pole pitch ratio is 1, where changing pole arc to pole pitch ratio, moving magnets and pole pairing can not be applied.

$$\begin{cases} \theta_a = \frac{2\pi\alpha_p}{(2p-1)k_t+1} \\ \theta_b = k_t\theta_a \end{cases}$$

Fig 5.8 gives the peak cogging torque with variation for three PMSMs, obtained by FEA which can give believable preciseness to calculations. Note that the three PMSMs here are carefully chosen and representative for studying thismethod, including 6-pole 48-slot (integer number of slots per pole), 8-pole 36-slot (fractional number of slots per pole) and 6-pole 27-slot (odd number of stator slots). From Fig 5.8, the peak cogging torque changes greatly with variation, where it achieves maximum when k_t=1 for all the three machines. When we have a 10% k_t variation i.e. k_t=0.9 and k_t=1.1, which is not a crucial change, the peak cogging torque for all the three machines has been reduced more than 50%.

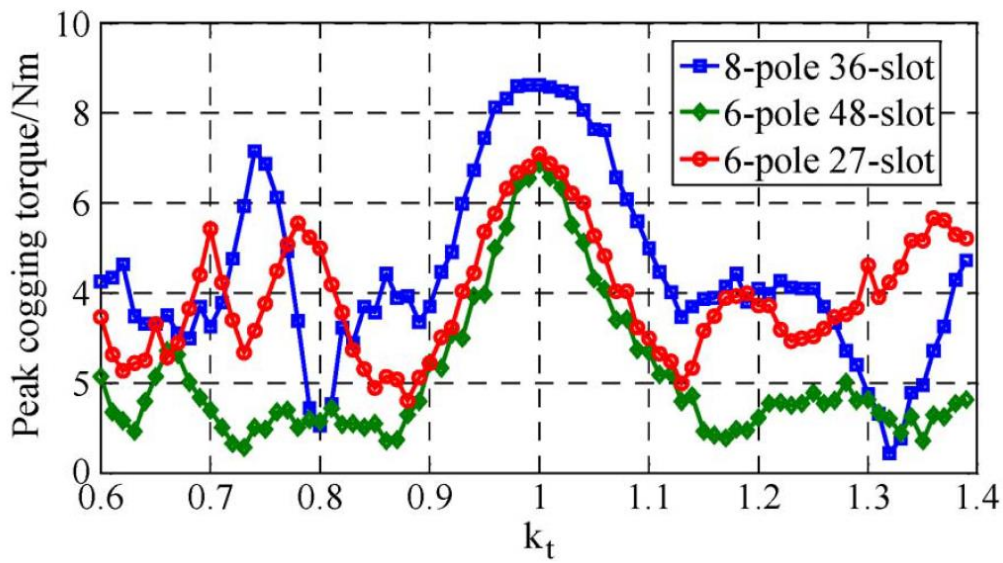

Fig 5.8 Peak cogging torque of three representative PMSMs with different which is calculated by FEA.

In this method, we examine the influence of the presented method on operation performance in terms of average torque, torque ripple and Unbalance Magnetic Pull (UMP), which not only influences the burden of machine bearings and rotor dynamics, but also contributes to noise and vibration. For the 24-pole 72-slot PMSM, the total torque ripple with k_t=1 at full load current on q-axis is 30.57%, which is a high value because this machine is not carefully designed where a simple single layer full pitch winding is used. However, the torque ripple is greatly reduced to be 2.73% and 2.49%

with k_t=0.715 and 1.628 which are the optimal value for minimizing cogging torque. Meanwhile, the average torque has a reduction of 4.62% and 4.49%, respectively. For the 6-pole 36-slot PMSM which uses double layer short pitch winding, the torque ripple with k_t=1 at full load current on q-axis is 17.26%, while the torque ripple with k_t=0.843 and 1.213 are both reduced to be 2.73% at a cost of average torque reduction of 0.58% and 0.62%, respectively[59]. In addition, this method is easy to realize in manufacturing and cost-saving compared to skewing, so it maybe of significant interest to the designer since it can simultaneously minimize cogging torque and suppress the operation torque ripple. However, the UMP experienced in both machines have been increased. This is mainly due to the asymmetric distribution of the magnets. So the mechanical burden of the machine bearing should be assessed when the method is applied.

5.5 Torque Ripple Reduction of Axial Flux Permanent Magnet Synchronous Machine with Segmented and Laminated Stator

Axial flux permanent magnet (AFPM) machines, which have unique characteristics such as high aspect ratio, high torque density and excellent efficiency, are becoming commodities in more and more applications, especially electrical tractions and propulsions. Recently, major efforts have been spent on advancing AFPM machine technologies for electric vehicle (EV) applications. A new AFPM machine, utilizing yokeless and segmented armature (YASA) topology and soft magnetic composite (SMC), is proposed to improve the torque density so, as to be essentially suitable for electric sports car propulsion. Instead, a novel AFPM using segmented and laminated steel stator is presented for in wheel direct drive EV application [60,61].

Torque quality of AFPM machines, which is directly related to the torque ripple components, is of particular-importance for in-wheel direct drive EV applications, since it could bring unpleasant drive experience. Torque ripple, which is the torque pulsation caused by the periodic components in the instantaneous torque of the machine, could result in severe mechanical vibration even failure. The torque ripple of PM synchronous machine comprises two different components, load dependent torque pulsation which arises from distortion of the sinusoidal back EMF and armature current, and cogging torque originating from the PMs' tendency to align themselves with the minimum reluctance path given by the relative position between rotor and stator which is unaffected by the load [62]. Primarily, the torque ripple problem in AFPM machines can be addressed by reducing cogging torque and minimize the back EMF harmonic contents from the design point of view. Alternatively, sophisticated control methods can also be employed to mitigate the torque ripple in PM synchronous machines. Nonetheless, it is worth pointing out that compromise is usually necessary to achieve the competing targets.

This topic presents a simple but efficient technique to mitigate the torque ripple in an AFPM synchronous machine with segmented and laminated stator based on shaping magnet pole. The design of the machine is intended for in wheel direct drive EV propulsion [63-66].

5.5.1 Axial flux permanent magnet synchronous machine with segmented and laminated stator

The AFPM machine under study in this paper has a rotor stator- rotor configuration, and comprises novel stator poles made of linearly proportionally sized laminated steel sheets stacked together to form a smooth laminated core. Each stator pole has concentrated windings embraced and is individually segmented and stacked together to form an integrated yokeless stator with maximum utilization of magnetic material by means of two high strength aluminum alloy ring holders. This structure thus shares number of typical merits with the YASA configuration: (a) shortened end windings leading to higher torque density and efficiency, (b) ease of winding process and high winding fill factor, (c) reduced mutual inductance between the machine phases resulting in improved phase independency and fault tolerance, and (d) reduced stator core weight and core losses due to the absence of the stator yoke. Additionally, this structure has some advantages over the YASA configuration: (a) increased magnetic loading and mechanical strength, (b) reduced cost due to the inexpensive lamination material, (c) improved efficiency as a result of reduced stator core losses. It should be highlighted that parallel stator slot openings, rather than radial slot openings, are employed in the proposed machine and as a consequence, the ratio of the width of the slot openings to the slot-pitch is not constant anymore. The key design parameters of the proposed machine are given in Table 5.3

5.5.2 Torque ripple assessment using an analytical approach

In general, the instantaneous torque output of a three phase PM synchronous machine without leakage inductance and magnetic saturation consideration can be given by

$$T_m(t) = \frac{e_a(t)i_a(t) + e_b(t)i_b(t) + e_c(t)i_c(t)}{\omega_r} + T_{cog}(t) \qquad \text{..... (5.1)}$$

In the electromagnetic and torque ripple analyses during the machine design stage of the proposed machine, it is assumed that the armature reaction is neglected, the phase currents are ideally sinusoidal and maintained in phase with the fundamental components of the corresponding phase back EMFs.

$$T_{em}(t) = \frac{E_1 I_1}{\omega_r} + \sum_{n=1}^{\infty} \frac{I_1\left(E_{6n+1} - E_{6n-1}\right)}{\omega_r} \cos\left(6n\omega_r t\right) \qquad \text{..... (5.2)}$$

PARAMETER	VALUE	UNIT
Stator pole number	12	-
Magnet pole number	10	-
Magnet outer radius	95	mm
Magnet inner radius	55	mm
Stator innermost layer	53.84	mm
Stator outermost layer	93	mm
Wingding axial length	39	mm
Winding thickness	9.4	mm
Magnet Material	NdFe40SH	-
Magnet angle span	30	degree
Magnet axial thickness	5	mm
Air gap axial length	1.5	mm
Stator slot opening width	4.1	mm
Stator pole shoe axial thickness	8	mm
Rated rotational speed	1200	rpm
Rated DC link Voltage	80	V
Rated torque output	50	N·m

Table 5.3 Key design parameters of the proposed machine

Meanwhile, the second one can be expressed as [67]

$$T_{cog}(t) = \sum_{n=1}^{\infty} T_n \sin\left(nN_c\omega_r t + \varphi_n\right) \qquad \text{..... (5.3)}$$

Since it is the least common multiple of the machine stator and rotor pole numbers, Nc is a multiple of 6. Thus, it can be inspected from equation (5.2) and (5.3) that the Instantaneous torque output contains an average component and harmonics of the order of six. It also can be observed that the back EMF and cogging torque are the main issues for the torque ripple reduction of the machine. In order to achieve adequate accuracy, a 3-D FEA model for machine optimization and design is always necessary. However, due to extensive computing time consumed, it is often not justified to develop complex 3-D FEA models at initial design stages. Therefore efficient but accurate analytical measures for back EMF and cogging torque estimations are of particular interest for quick determination of a feasible range including the optimal design. As a complement, the 3-D FEA are eventually carried out to determine the final optimal design. An approximated 3-D analytical model can be developed through extending exact slot less two-dimensional (2-D) model by a simple but effective dependence modeling of the no load magnetic field [68-70]. Consequently, the instantaneous value of the no load magnetic field density in the air gap near stator pole of the machine can be obtained by

$$B(r,\theta) = B_{slotless}(r,\theta)\,\xi(r,\theta)\,\tau(r) \qquad \text{..... (5.4)}$$

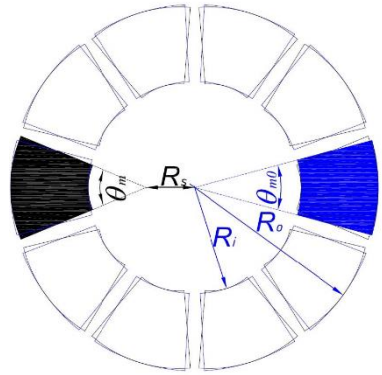

Fig 5.9 Rotor magnet optimization and arrangements

The back EMF, no load induced voltage by the magnets only, can be evaluated from the air gap flux density distribution near stator poles. Here, the back EMF of individual coil is computed by the time derivative of the flux linkage through the corresponding stator pole as follow

$$e_{coil}(t) = N_{coil}\lambda \frac{d}{dt}\int_{R_i}^{R_o}\int_{\omega_r t-\frac{(1-\alpha_s(r))\pi}{p_s}}^{\omega_r t+\frac{(1+\alpha_s(r))\pi}{p_s}} B(r,\varphi)\xi(r,\varphi)\tau(r)\,r\,dr\,d\varphi. \qquad \text{..... (5.5)}$$

Then the phase back EMF of the machine can be synthesized as

$$e_{phase}(t) = \frac{1}{m}\sum_{i=K} e_{coil}\left(t+\frac{2i\pi}{p_s}\right) \qquad \text{..... (5.6)}$$

System level optimization of torque quality with all parameters involved is made possible with significant time saving by the proposed analytical approach. Torque ripple improvement in AFPM with segmented and laminated stator using magnet shape optimization is an effective and low-cost design approach but requires careful selection of magnet span angle. The analysis is complicated due to machine saturation induced nonlinearities at full load condition.[71] The results show that the torque ripple of the proposed machine can be significantly reduced by the proposed magnet design technique which would not deteriorate the machine performance and increase the manufacture cost.

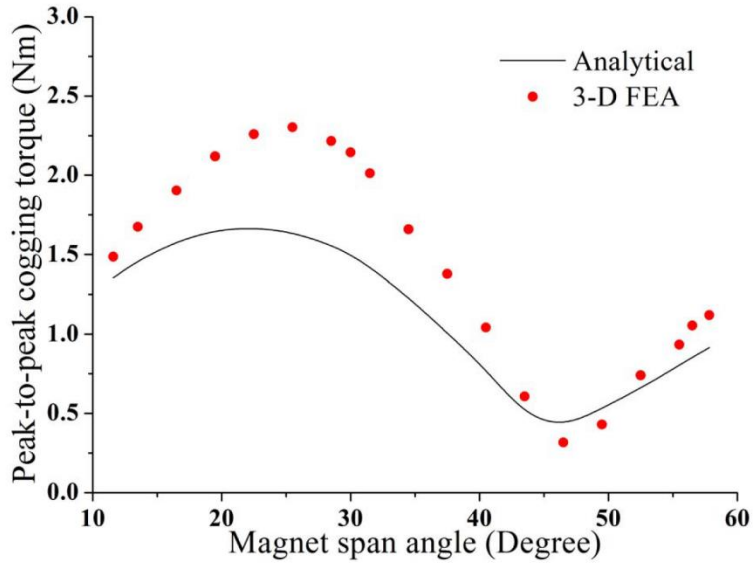

Fig 5.10 Peak-to-peak values of cogging torque for different magnet shapes

The comparison of peak-to-peak cogging torque variation is illustrated in Fig 5.10. The results manifest that the magnet shape has a significant impact on the cogging torque.
The shape of cogging torque profiles from analytical evaluations is almost same as the one from 3-D FEA. From Fig 5.10, on the other hand, considerable deviations between the peak-to-peak cogging torque values from the analytical and 3-D FEA results can be observed, for the reason that the analytical model is developed based on an approximate geometric shape of the stator pole shoe instead of the actual irregular one. However, the maximum and minimum amplitudes of both the approaches occur at the approximately same magnet span angles. The polarity of the cogging torque alters when the magnet span angle crosses the minimum trough, nearly 46 degree, where the optimal magnet span angle for cogging torque suppression can be found. Consequently, it is verified that the analytical model is sufficient enough to determine a small and feasible magnet angle span range including optimal magnet shape with massive computing time saving. It can be seen that the average torque outputs remain at around 1% due to nearly unchanged fundamental components of back EMF. Torque ripples, however, varies from almost 4% to more than 12% within the whole magnet span angle range. Although 50 degree is not the optimal magnet span angle for cogging torque, neither for back EMF, it gives optimal overall torque ripple of 4.2%, which is much lower than the 9.3% found in the original magnet of 30 degree. The torque profiles of the machine with 30 and 50 degree magnets from 3-D FEA are demonstrated in Fig. 10, which has revealed that the torque pulsations are remarkably reduced by utilizing the optimal magnet span angle. [71]

CONCLUSION

The permanent magnet machines are an attractive solution for compact machines with higher efficiency and higher torque-to-volume ratio. Such machines are now in great demand in many applications including the automotive steering application. These applications also require quiet machine operations, which mean a lower level of cogging torque and torque ripple and reduced noise and vibration. The key requirements for quiet operation have been identified as cogging torque, torque ripple, and unbalanced radial forces; the research objectives to address these issues have been outlined in the introductory chapter. The design-based methods for improving cogging torque, torque ripple and radial vibration were discussed in detail. The design methodology was utilized to develop analytical designs for four different motor topologies with different slot/pole combinations. Analytical design obtained for these motor configurations were for a given common set of performances and design constraints. FE analysis was also carried to validate the results of the analytical models. An example design showed the effectiveness of these analytical models in predicting the performance of the machines. Both FEA and test results are included to show the comparison for several PMSM configurations. The effect of slot/pole combinations and magnet shapes on the magnitude and harmonic content of torque waveforms in a PMSM drive have been studied. Finite element analysis (FEA) and experimental results show that for certain magnet designs and a configuration skewing does not necessarily reduce the ripple in the electromagnetic torque but may cause it to increase. Here by seeing many techniques that prompt the reduction of the cogging torque and torque ripple analysis we knew that every method has some drawbacks in reducing effectively in Surface mounted permanent magnet synchronous machines and in interior permanent magnet synchronous machines. Discussion of every single technique was done and finally by using asymmetric flux barriers technique with the finite element method we it is able to reduce cogging torque and torque ripple effectively using few configurations of flux barriers. There are further new techniques being introduced and development in the existed techniques are being done.

BIBLIOGRA1PHY

1. History of Interior Permanent Magnet Motors- Md Azizur Rahman
2. Permanent magnet synchronous motor-Dmitry Levkin
3. IEEE Standard 141-1993 Recommended Practice for Electric Power Distribution for Industrial Plants
4. Tesla's top motor engineer talks about designing a permanent magnet machine for Model 3
5. New Methods for Reducing the Cogging Torque and Torque Ripples of PMSM- Gurakuq Dajaku1) and Dieter Gerling2), IEEE
6. S. M. Hwang, et. al., "Various design techniques to reduce cogging torque by Controlling energy variation in permanent magnet motors," IEEE Transactions on Magnetics, pt. 1, vol. 37, pp. 2806-2809, Jul. 2001.
7. D. C. Hanselman, Brushless Permanent Magnet Motor Design, Writers' collective, Cranston, Rhode Island, 2003.
8. P. Vas, Sensorless Vector and Direct Torque Control, Oxford university press, New York, 1998.
9. L. Yong, J. Zou, L. Youngping, "Optimum design of magnet shape in permanentmagnet synchronous motors," IEEE Transaction on Magnetics vol. 39, no. 6,Nov 2003.
10. S. Huang, M. Aydin, T. A. Lipo, "Torque quality assessment and sizing optimizing for surface mounted permanent magnet machines," IEEE Industry Application Society, Sept. 2001.
11. S. M. Hwang and D. K. Lieu, "Reduction of torque ripple in brushless dc motors,"IEEE Transactions on Magnetics, pt. 2, vol. 31, pp. 3737-3739, Nov. 1995.
12. A. Murray, "Torque and EMF ripple reduction in brushless machines," IEEE Colloquium on Permanent Magnet Machines and Drives, vol. 1, pp. 8/1-8/4, Feb.1993.
13. A. Carlo, C. Domeniko, A. Cristofolini, M. Fabbri, G. Serra, "Application of a multi-objective minimization technique for reducing the torque ripple in permanent-magnet motors," IEEE Transaction on Magnetics, vol. 35, no. 5, Sept 1999.
14. J. F. Gieras, C. Wang, J. C. Lao, Noise of Polyphase Electric Motors, Taylor & Rancis group, Boca Raton, FL, 2006.

15. M. Dai, A. Keyhani, and T. Sebastian, “Torque ripple analysis of a PM brushless DC motor using finite element method,” IEEE Transaction on Energy Conversion, vol.19, pp. 40-45, Mar. 2004.
16. N. Boules, H. Rassem, N. Chandra, T. W. Nehl, L. Bruno, C. Shaotang., “Torque ripple free electric power steering motor,” US Patent No. 6,498,451 , 1995.
17. M. Brackley and C. Pollock, “Analysis and reduction of acoustic noise from a brushless DC drive,” IEEE Transactions on Industry Applications, issue 3, vol. 36, pp. 772-777, May-Jun. 2000.
18. P.L. Timar, Noise and Vibration of Electrical Machines, Elsevier, Sept. 2004.
19. D. W. Novotny and T.A. Lipo, Vector Control and Dynamics of AC Drives, Clarendon press, Oxford, 1997.
20. D. E. Cameron, J. H. Lang, S. D. Umans, “The origin of acoustic noise in variable-reluctance motors,” IEEE Trans. on Industry Applications, vol. 28, no. 6, pp.1250-1255, Nov./Dec. 1992.
21. R. Belmans, K. J. Binns, W. Geysen and A. Vandenput, Vibrations and audible noise in alternating current machines, Kluwer Academic Publishers, NATO ASI series, 1988.
22. P. Vijayraghavan and R. Krishnan, “Noise in electric machines: A review,” IEEE Transactions on Industry Applications, vol. 35, no.5, pp. 1007-13, Sept.-Oct.,1999.
23. J. F. Gieras and M. Wing, Permanent Magnet Motor Technology, Marcel Dekker Inc., New York, 2002.
24. N. Bianchi and S. Bolognani, “Design techniques for reducing cogging torque in surface-mounted PM motors,” IEEE Transactions on Industry Application Society, issue 5, vol. 38, pp. 1259-1265, Sept-Oct. 2002.
25. V. Petrovic, et. al., “Design and implementation of an adaptive controller for torque ripple minimization in PM synchronous motors,” IEEE Transactions on Power Electronics, vol. 5, pp. 871-880, Sept. 2000.
26. C. Breton, J. Bartolome, J. A. Benito, G. Tassinario, I. Flotats, C. W. Lu, B. J. Chalmers , “Influence of machine symmetry on reduction of cogging torque in permanent-magnet brushless motors,” IEEE Transactions on Magnetics, vol. 36, pp. 3819-3823, Sept. 2000.
27. N. Boules, H. Rassem, N. Chandra, T. W. Nehl, L. Bruno, C. Shaotang., “Torque ripple free electric power steering motor,” US Patent No. 6,498,451 , 1995.
28. Y. K Chin, W. M. Arshad, T. Backstrom, C. Sadarangani, “Design of a compact BLDC motor for transient applications,” IEEE Electric Machines and , IEMDC, pp. 743-747, June 2001

29. Y. Keno, N. Matsui, “A design approach for direct-drive permanent magnet motors,” 40th IEEE Industry Application Conference, vol. 1, pp. 245-252, Oct. 2005.
30. D. C. Hanselman, Brushless Permanent Magnet Motor Design, Writers’ collective, Cranston, Rhode Island, 2003.
31. S. M. Hwang, et. al., “Various design Transactions on Magnetics techniques to reduce cogging torque by controlling energy variation in permanent magnet motors,” IEEE, pt. 1, vol. 37, pp. 2806-2809, Jul. 2001.
32. D. C. Hamselman, “Minimum torque ripple, maximum efficiency excitation of brushless permanent magnet motors,” IEEE Transactions on Industrial Electronics, vol. 41, pp. 292-300, June 1994.
33. B. Grcar, P. Cafuta, G. Stumberger, A. M. Stankovic, “Control based reduction of pulsating torque for PMAC machines,” IEEE Transactions on Energy Conversions, vol. 17, no. 2, Jun. 2002.
34. B. Grcar, P. Cafuta, G. Stumberger, A. M. Stankovic, “Control based reduction of pulsating torque for PMAC machines,” IEEE Transactions on Energy Conversions, vol. 17, no. 2, Jun. 2002.
35. F. Taegen and J. Kolbe, “Vibrations and noise produced by special purpose permanent-magnet synchronous motors in variable frequency operation,” IEEE International Conference on Power Electronics and Drive Systems, vol. 2, pp. 583-588, Oct. 2001.
36. G. Jiao, C. D. Rahn, “ Field weakening for radial force reduction in brushless permanent-magnet DC motors,” IEEE Transactions on Magnetics, issue 5, vol. 40, pp. 3286-3292, Sept. 2004.
37. I. Husain, Electric and Hybrid Vehicles: Design Fundamentals, CRC press, Boca Raton, FL 2003.
38. R. Carlson, A. A. Tavares, J. P. Bastos, M. L. Mazenc, “Torque ripple attenuation in permanent magnet synchronous motors,” IEEE Industry Application Society, vol. 1, pp. 57-62, Oct. 1989.
39. M. Joran, “Modeling and control design of VSI-fed PMSM drive systems with active load,” 12th Annual Conference Proceedings of APEC, vol.2, pp. 728-735, Feb. 1997.
40. D. Ishak, Z. Q. Zhu, D. Howe, “Unbalanced magnetic forces in permanent magnet brushless machines with diametrically asymmetric phase windings,” 40th IEEE Industry Application Conference, vol. 2, pp. 1037-1043, Oct. 2005.

41. F. Magnussen and H. Lendenmann, “Parasitic effects in PM machine with concentrated windings,” 40th Industry Application Society Annual Meeting, vol. 2, pp. 1044-1049, Oct. 2005
42. M. N. Anwar, Design of switched reluctance machines for low-acoustic noise and wide speed range operation, Dissertation presented to the graduate faculty of the University of akron, 2001.
43. H. Cho, H. R. Cho, H. Lee, “Effect of pole to slot number ratio on back-emf constant of BLDC motor with non-overlapping stator winding,” International Electric Machines & Drives Conf., pp. 54-56, 1999.
44. H. Cho, H. R. Cho, H. Lee, “Effect of pole to slot number ratio on back-emf constant of BLDC motor with non-overlapping stator winding,” International Electric Machines & Drives Conf., pp. 54-56, 1999.
45. D. A. Staton and S. Eric, “Computer aided design of brushless servo motors,” UK Magnetic Society Seminar, Nov. 2000.
46. N. Bianchi and S. Bolognani, "Design techniques for reducing the cogging torque in surface-mounted PM motors," IEEE Transactions on Industry Applications, vol. 38, pp. 1259-1265, 2002.
47. L. Dosiek, P. Pillay, “Cogging torque reduction in permanent magnet machines”, IEEE Transactions on Industry Application, Vol. 43, No. 6, 2007.
48. C. S. Koh and J. S. Seol, "New cogging-torque reduction method for brushless permanent-magnet motors," IEEE Transactions on Magnetics, vol. 39, pp. 3503 3506, 2003.
49. C. Xia, Z. Chen, T. Shi, and H. Wang, "Cogging Torque Modeling and Analyzing for Surface-Mounted Permanent Magnet Machines With Auxiliary Slots," IEEE Transactions on Magnetics, vol. 49, pp. 5112-5123, 2013.
50. W. Ren, Q. Xu, Q. Li, and L. Zhou, "Reduction of Cogging Torque and Torque Ripple in Interior PM Machines With Asymmetrical V-Type Rotor Design," IEEE Transactions on Magnetics, vol. 52, pp. 1-5, 2016.
51. Tanwei Zhou, and Jian-Xin Shen-Cogging Torque and Operation Torque Ripple Reduction of Interior Permanent Magnet Synchronous Machines by Using Asymmetric Flux-Barriers
52. P. Ponomarev, I. Petrov, and J. Pyrhonen, “Influence of travelling current linkage harmonics on inductance variation, torque ripple and sensor less capability of tooth-coil permanent-magnet synchronous machines,” IEEE Trans. Magn., vol. 50, no. 1, Jan. 2014, Art. ID 8200108.
53. J. Sopanen, V. Ruuskanen, J. Nerg, and J. Pyrhonen, “Dynamic torque analysis of a wind turbine drive train including a direct-driven permanent-magnet

generator," IEEE Trans. Ind. Electron., vol. 58, no. 9,pp. 3859–3867, Sep. 2011.

54. I. Petrov and J. Pyrhonen, "Performance of low-cost permanent magnet material in PM synchronous machines," IEEE Trans. Ind. Electron., vol. 60, no. 6, pp. 2131–2138, Jun. 2013.
55. Y. Alexandrova, R. Semken, and J. Pyrhönen, "Permanent magnet synchronous generator design solution for large direct-drive wind turbines," Int. Rev. Elect. Eng., vol. 8, no. 6, p. 1728, 2013.
56. P. Ponomarev, P. Lindh, and J. Pyrhonen, "Effect of slot-and-pole combination on the leakage inductance and the performance of tooth-coil permanent-magnet synchronous machines," IEEE Trans. Ind. Electron., vol. 60, no. 10, pp. 4310–4317, Oct. 2013.
57. W. Q. Chu and Z. Q. Zhu, "Investigation of torque ripples in permanent magnet synchronous machines with skewing," IEEE Trans. Magn., vol. 49, no. 3, pp. 1211–1220, Mar. 2013.
58. Ilya Petrov, Pavel Ponomarev, Yulia Alexandrova, and Juha Pyrhönen Unequal Teeth Widths for Torque Ripple Reduction in Permanent Magnet Synchronous Machines With Fractional-Slot Non-Overlapping Windings
59. Daohan Wang , Xiuhe Wang , and Sang-Yong Jung Cogging Torque Minimization and Torque Ripple Suppression in Surface-Mounted Permanent Magnet Synchronous Machines Using Different Magnet Widths
60. T. J. Woolmer, and M. D. McCulloch, "Axial-flux permanent magnet machines: a new topology for high performance applications," in proc. IET Hybrid Vehicle Conference, 2006, pp. 27-42.
61. T. J. Woolmer, and M. D. McCulloch, "Analysis of the yokeless andsegmented armature machine," in proc. IEEE International Electric machines and drives conference, 2007, pp. 704-708.
62. W. Fei, P. C. K. Luk, and K. Jinupun, "A new axial flux permanentmagnet segmented-armature-torus machine for in wheel direct drive applications," in proc. IEEE Power Electronics Specialists Conference, 2008, pp. 2197-2202.
63. M. Aydin, " Magnet skew in cogging torque minimization of axial gap permanent magnet motors," in proc. Inter. Conf. Electrical Machines, 2008, paper ID 1186 (1-6).
64. F. Caricchi, F. Crescimbini, G. Capponi, and L. Solero, "A novel solidstate-commutator PM motor arrangement for EV application," in proc. IEEE IAS Annu. Meeting, 1999, pp. 2545-2551.

65. V. Petrovic, R. Ortega, A. M. Stankovic, and G. Tadmor, " Design and implementation of an adaptive controller for torque ripple minimization in PM synchronous motors," IEEE Trans. Power Electron., vol. 15, no. 5, pp. 871-880, Sept. 2000.
66. M. Dai, A. Keyhani, and T. Sebastian, "Torque ripple analysis of a PM brushless DC motor using finite element method," IEEE Trans. Energy Convers., vol. 19, no. 1, pp. 40-45, Mar. 2004.
67. M. Aydin, Z. Q. Zhu, T. A. Lipo, and D. Howe, "Minimization of cogging torque in axial-flux permanent-magnet machines: design concepts," IEEE Trans. Magn., vol. 43, no. 9, pp.3614-3622, Sept. 2007
68. A. Parviainen, M. Niemela, and J. Pyrhonen, "Modeling of axial flux permanent-magnet machines," IEEE Trans. Ind. Applicat., vol. 40, no. 5, pp. 1333-1340, Sept./Oct. 2004.
69. P. Kurronen, and J. Pyrhonen, "Analytic calculation of axial-flux permanent-magnet motor torque," Proc. IET – Electr. Power Appl., vol. 1, no. 1, pp. 59-63, Jan. 2007.
70. W. Fei, and P. C. K. Luk, "Performance study of two axial-flux permanent-magnet machine topologies with soft magnetic composite cores," in proc. IEEE 6th Inter. Power Electron. And Motion Control Conf., 2009, pp. 411-417.
71. W. Fei, and P. C. K. Luk Torque Ripple Reduction of Axial Flux Permanent Magnet Synchronous Machine with Segmented and Laminated Stator.
72. R.Suja, P.Melba Mary, "Minimization Of Torque Ripples In Permanent Magnet Synchronous Motor-Overview" , International Journal Of Scientific & Engineering Research, Volume 4, Issue 10, October-2013.
73. "Simple Method of Torque Ripple Minimization and performance Characteristics Enhancement of Fuel Cell based PMSM Drive" , International Journal of Computer Applications (0975 – 8887) Volume 19– No.2, April 2011.
74. L. Romeral, A. Fabrega, J. Cusido, A. Garcia, J.A. Ortega ,"Torque Ripple Reduction in a PMSM driven by Direct Torque Control" IEEE Transactions 2008.